Supplementary information

Photoactive Fe(III)pyclen complexes for light-driven aerobic oxidation of *p*-xylene

Matteo Alberti,[a] Greta Rossi,[b] Djihed Boucherabine,[a] Fausto Cargnoni,[c]* Mario Italo Trioni,[c] Giulia Taini,[a] Dominika Zakutna,[d] Arianna Gentilin,[b] Luka Đorđević,[b] Andrea Sartorel[b]* and Alessandro Caselli[a c]*

[a]Department of Chemistry, Università degli Studi di Milano, via Golgi 19, 20133 Milano, Italy. E-mail: alessandro.caselli@unimi.it ; phone: +39 02 50314372.

[b]Department of Department of Chemical Sciences, University of Padova, via Marzolo 1, 35131 Padova, Italy. E-mail: andrea.sartorel@unipd.it

[c]Istituto di Scienze e Tecnologie Chimiche "G. Natta" CNR-SCITEC via Golgi 19, 20133 Milano, Italy. E-mail: fausto.cargnoni@scitec.cnr.it

[d]Department of Inorganic Chemistry, Charles University, Hlavova 2030/8 128 40, Prague 2, Czech Republic.

*Correspondence: Alessandro Caselli
alessandro.caselli@unimi.it

Andrea Sartorel
andrea.sartorel@unipd.it

Fausto Cargnoni
fausto.cargnoni@scitec.cnr.it

Table of contents

General remarks

All chemicals were commercially available and used as received except where specified. Acetonitrile and methanol were distilled over calcium hydride. Diethyl ether and hexanes were distilled over sodium/benzophenone. $CDCl_3$ for NMR analysis was passed through a basic alumina column and subsequently thoroughly degassed with several freeze-pump-thaw cycles. ^1H NMR analyses were performed with 400 MHz spectrometers at room temperature. The coupling constants (*J*) are expressed in hertz (Hz), and the chemical shifts (δ) in ppm. Catalytic tests were analyzed by gas chromatography. Magnetization measurements were performed at a physical property measurement system (PPMS) from Quantum Design equipped with a Vibrating Sample Magnetometry (VSM) module. Mössbauer spectroscopy of ^{57}Fe was carried out on a Wissel spectrometer using transmission geometry and a proportional detector at ambient temperature without a magnetic field. An α-Fe foil is used as standard, and spectra fitting is carried out using the Wissel NORMOS routine. UV spectra were recorded at 20 °C. Mass spectra of the complexes were acquired with a Waters Q-ToF SYNAPT G2-Si HDMS 8K high resolution mass spectrometer by the Unitech COSPECT laboratory. Elemental analyses were carried out at the University of Milan. Microwave enhanced reactions were conducted in a Biotage® Initiator+ microwave synthesizer. 2,6-bis(methanesulfonyloxymethyl)pyridine was synthesized according to our previously reported methods.[1] The optimized synthesis of the pyclen ligand, 3,6,9-triaza-1(2,6)-pyridinacyclodecaphane, is detailed below. Pure iron(III) trifluoromethanesulfonate was prepared following a slightly modified literature-reported method,[2] working under anaerobic and anhydrous conditions using typical Schlenk techniques.

Synthetic procedures

Synthesis of the ligand and precursors

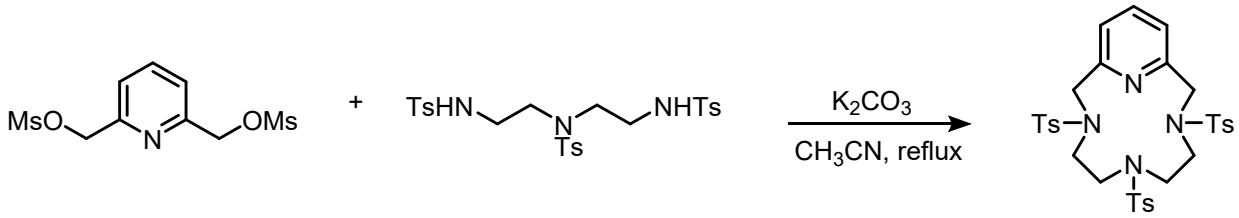

3,6,9-tritosyl-3,6,9-triaza-1(2,6)-pyridinacyclodecaphane. In an oven-dried round bottom flask, 2 g of anhydrous potassium carbonate (14.5 mmol) were kept under vacuum for 1 h at a temperature of 120°C. Afterwards, the solid was cooled to 30°C, and 2.72 g of commercially available 1,4,7-tritosyl-1,4,7-triazaheptane (4.81 mmol) were added along with 140 mL of dry acetonitrile. A solution containing 1.42 g of mesyl-protected pyridine-2,6-diyldimethanol (4.81 mmol) in 60 mL of dry acetonitrile was then added dropwise. The suspension was then brought to the boiling point and refluxed for 3 hours with vigorous agitation. At the end, the solvent was removed in vacuo and the solid residue was dissolved in DCM/H_2O (60 + 60 mL). The product was extracted three times with DCM (60 mL). The organic phases were washed once with brine, combined, and dried over sodium sulphate. The solution was filtered and the solvent was removed in vacuo. The product was recovered pure in a 96% yield. Characterization data agreed with published material.[1,3] ^1H NMR (400 MHz, $CDCl_3$): δ 7.77 – 7.71 (m, 5H), 7.65 (d, J = 8.3 Hz, 2H), 7.43 (d, J = 7.7 Hz, 2H), 7.34 (d, J = 8.1 Hz, 4H), 7.27 (d, J = 7.9 Hz, 2H), 4.30 (bs, 4H), 3.33 (t, J = 7.5 Hz, 4H), 2.75 (bs, 2H), 2.45 (s, 6H), 2.41 (s, 3H).

3,6,9-triaza-1(2,6)-pyridinacyclodecaphane. The deprotection of *N*-tosylated pyclen was improved upon our last report[4] by using microwave enhanced synthesis. This method achieved better reproducibility and improved reaction times compared to thermal heating, as well as a sharp reduction of reaction temperature (from 250 C to 120 C) which resulted in an overall cleaner reaction. In a microwave vial, 2 g of 3,6,9-tritosyl-3,6,9-triaza-1(2,6)-pyridinacyclodecaphane (3 mmol) were suspended in 8 mL of concentrated sulfuric acid. The vial was sealed and then heated to 120° with microwave radiation. After 35 minutes, the solution was cooled to 0° and 100 mL of

diethyl ether were added under slow stirring. The gum-like precipitate was decanted and the supernatant is removed. The solid was dissolved in 20 mL of water and basified with NaOH pellets until pH 14 was reached. The product was then extracted with DCM, until the organic phases contained no product (it can be checked with a TLC plate). The gathered organic phases were then collected, quickly dried with sodium sulfate and the solvent was evaporated. The product was recovered pure in an 88% yield. Characterization data agreed with published material.[5] ^{1}HNMR (400 MHz, $CDCl_3$): δ 7.51 (t, J = 7.6 Hz, 1H), 6.99 (d, J = 7.6 Hz, 2H), 3.96 (s, 4H), 2.93 (bs, 3H), 2.74 – 2.66 (m, 4H), 2.27-2.20 (m, 4H).

Iron (III) triflate. Iron(III) trifluoromethanesulfonate was prepared following a slightly modified literature reported method, working under anaerobic and anhydrous conditions using typical Schlenk techniques.[2] Briefly, 2 g of anhydrous iron(III) chloride were transferred to an oven dried Schlenk flask and 5 mL of thionyl chloride were carefully added. The solid was stirred under reflux overnight to ensure the total elimination of water. Then, it was filtered under dinitrogen atmosphere and washed with two 5 mL portions of distilled hexanes. The solid was then gathered in a 50 mL Schlenk flask which was equipped with a stirring bar and a distilling bridge. In another flask, 40 mL of trifluoromethanesulfonic acid were stirred with 1 mL of trifluoromethanesulfonic anhydride for 30 minutes. Then, the acid was distilled under static vacuum onto the anhydrous iron(III) chloride. The mixture was then stirred at 150°C for 8 hours and under reflux conditions for 32 hours. The temperature was raised gradually to avoid unreacted iron(III) chloride disproportionation to iron(II) chloride and elemental chlorine.[6] The product is insoluble in acid, thus it was filtered and washed with freshly distilled trifluoromethanesulfonic acid. The solid was then dried by heating under vacuum at 50°C. Yield: 76%. *Anal. calcd.* for $FeC_3F_9S_3O_9$: C, 7.16; H, 0.00; N, 0.00; S,19.12; found: C, 9.72; H, 1.06; N, 0.00; S, 17.54.

Synthesis of complexes **1a-c**

All the procedures were carried out in anaerobic and anhydrous conditions in N_2 atmosphere using typical Schlenk techniques.

Synthesis of 1a. In an oven-dried Schlenk flask, 202 mg of pyclen (0.979 mmol) were dissolved in 15 mL of dry acetonitrile. The flask was heated gently to promote the full dissolution of the ligand. In another flask, 264.9 mg of commercially available $FeCl_3 \cdot 6\ H_2O$ (0.980 mmol) were dissolved in 5 mL of dry acetonitrile; this solution was then transferred dropwise to the first one. A greenish-brown precipitate immediately formed. The suspension was then refluxed for 2 hours, during which the precipitate turned bright yellow. Afterwards, the precipitate was filtered under dinitrogen atmosphere, and the product was washed with *n*-hexane. Yield: >99%. Anal. found: C, 36.17; H, 4.91; N, 15.14; calcd. for $C_{11}H_{18}Cl_3FeN_4$: C, 35.85; H, 4.92; N, 15.20. MS (ESI) *m/z* 332.06 ([M^+], 100%), $C_{11}H_{18}Cl_2FeN_4$ requires 332.03. HR-MS (ESI) *m/z* 330.0296 ([M^+], 10%), 295.00616 (100, [M^+-Cl]); $C_{11}H_{18}Cl_2FeN_4$ requires 330.0305; $C_{11}H_{18}ClFeN_4$ requires 295.0616.

Synthesis of 1a'. Suitable crystals for X-ray diffraction were grown by layering diethyl ether over a methanolic solution of **1a** (v/v = 2:1).

Synthesis of 1b. In an oven-dried Schlenk flask, 260 mg of pyclen (1.26 mmol) were dissolved in 15 mL of dry acetonitrile. The flask was heated gently to promote the full dissolution of the ligand. In another flask, 373 mg of anhydrous $FeBr_3$ (1.26 mmol) were dissolved in 6 mL of dry acetonitrile; this solution was then transferred dropwise to the first one. A dark red precipitate immediately formed. The suspension was then heated at 60°C for one hour. Afterwards, the precipitate was filtered under dinitrogen atmosphere and the product was washed with *n*-hexane. Yield: 75%. Anal. found: C, 26.05; H, 3.58; N, 10.83; calcd. for $C_{11}H_{18}Br_3FeN_4$: C, 26.33; H, 3.62; N, 11.16. MS (ESI) *m/z* 421.95 ([M^+] 40%), $C_{11}H_{18}Br_2FeN_4$ requires 421.92. HR-MS (ESI) *m/z* 339.0111 ([M^+-Br] 70%); $C_{11}H_{18}FeN_4Br$ requires 339.0118.

Synthesis of 1c. In an oven-dried flask, 76 mg of pyclen (0.37 mmol) were dissolved in 5 mL of dry acetonitrile. The solution was then heated gently to favor the full dissolution of the ligand. In another flask, 176 mg of $Fe(OTf)_3$

(0.350 mmol) were dissolved in 5 mL of dry acetonitrile. The resulting solution was added dropwise to the ligand solution. A sharp change from pale yellow to brown was noticed. The solution was left stirring under gentle heating (external bath temperature of 50°C) for one hour. Afterwards, the volume of the solution was halved under vacuum, and the flask was left overnight at -20°C. The solution was then filtered to remove any eventual unreacted ligand. Layering with dry diethyl ether to attempt the crystallization of the product did not yield any crystalline material, and most of the product remained in solution. The solvent was thus removed under vacuum to yield an oily residue, which was rendered solid by freezing and thawing it under vigorous stirring in dry diethyl ether. The product was obtained as a powdery brown precipitate, which was filtered and washed with dry diethyl ether. Yield: >99%. Anal. found: C, 24.04; H, 3.02; N, 7.75; S, 13.26; calcd. for $C_{14}H_{18}F_9FeN_4O_9S_3$: C, 23.71; H, 2.56; N, 7.90; S, 13.56. MS (ESI) *m/z* 411.04 ([M^+-OTf] 100%); $C_{12}H_{18}F_3FeN_4O_3S$ requires 411.04. HR-MS (ESI) *m/z* 411.0396 ([M^+-OTf] 100%); $C_{12}H_{18}F_3FeN_4O_3S$ requires 411.0401.

General photocatalytic procedures

Photochemical experiments for the oxidation of *p*-xylene were conducted in 8 mL commercial glass vials, using a homemade photoreactor with 16 positions irradiating from the bottom of the vial with white light (33 mW/cm^2 corresponding to 0.33 sun intensity), or with blue LED at 405 nm. Typical conditions employed 1 mL of a solution of 80 mM *p*-xylene and 2.5 mM iron catalyst under stirring (400 rpm). For quantum yield determination, a blue LED emitting at 405 nm was employed, and the fraction of absorbed photons was estimated with a power meter, by subtracting the emission intensity in the absence and in the presence of the reaction solution. Identification and quantification of the products was performed by ^{1}H-NMR by comparison with commercial chemicals and by adding mesitylene as an internal standard.

Electron Paramagnetic resonance (EPR) spectra were acquired on a Bruker ESR5000 operating at a microwave frequency of 9.4 GHz. 25 µL of solution samples containing BMPO spin trap (50 mM) were introduced into capillaries. The spectra were recorded using ESRStudio at room temperature with 20 mT microwave power, 0.1 mT modulation and 360 seconds sweep time. The sample was irradiated *in situ* using 405 nm LED for 60 seconds.

Crystal structure determination

Single crystal X-ray diffraction data were collected with a XtaLAB Synergy S diffractometer (Rigaku). The radiation source was a micro-focus sealed X-ray tube with copper radiation (Cu-Kα, λ = 1.54184 Å) with the generator working at 50 kV and 1 mA. Data collection, frame integration, and data reduction were carried out with CrysAlis Pro version 1.171.42.54a[7] using an empirical absorption correction with spherical harmonics (SCALE3 ABSPACK). The structure was solved by dual space methods with SHELXT-2015[8] and refined with SHELXL-2018 using the WinGX program suite.[9] Structure refinement was done using full-matrix least-square routines against F2. Hydrogen atoms were modelled on idealized positions.

Theoretical calculations

Calculations on **1a**, **1b** and **1c** were performed within the Density Functional Theory (DFT) approach, as implemented in the Gaussian09 code (revision D.01). Total energies and wavefunctions have been determined using the OPBE functional for the description of exchange and correlation terms. Indeed, this functional proved to be effective in predicting the correct energy distribution of several spin states of iron complexes.[10,11] All atoms have been assigned the 6-31G(d,p) localized basis set, whose polarization Gaussian functions are capable of describing accurately the deformation of the wavefunction with respect to the spherical atomic arrangement. The properties of **1a**, **1b**, and **1c** have been computed considering just the cation, since the counterion is likely to act mostly as a pure electrostatic Coulomb term. In all systems, the geometry of the moiety has been fully optimized, and its total energy has been corrected, including the zero-point vibrational contribution. We studied **1a**, **1b**, and **1c** either in the gas phase or dispersed in acetonitrile as the solvent. We accounted for the effects of solvation with the implicit Solvation Model based on Density scheme.[12] We considered three different spin states in all systems, corresponding to the three reasonable arrangements of electrons in the partially filled *d* shell of the iron atom. We therefore studied low, medium, and high spin states, where the number of unpaired electrons amounts to 1, 3, and

5, respectively. Homolytic fragmentation of **1a**, **1b**, and **1c** has been simulated by removing one ligand from the central Fe atom, reoptimizing the geometry and rearranging the electronic spin accordingly (in this case we tested four possible numbers of unpaired electrons: 0, 2, 4, and 6). In studying the fragmentations of the complexes, we evaluated the stability of the Cl•, Br• and OTf• radicals by means of Coupled Cluster and Configurations Interaction calculations at the CCSD and the CISD levels of theory, respectively.
To assess the quality of DFT computations on **1a**, **1b** and **1c**, we also performed a series of tests on gas-phase systems. First, we assigned the cc-pVTZ set for all atoms and, second, we verified the stability of results using the range-separated ωB97X hybrid functional, which performs well in the case of Fe(III) complexes.[13-15] The picture based on OPBE/6-31G(d,p) does not change significantly at varying basis set and functional, suggesting that our approach is appropriate for the moieties under investigation.

To simulate the experimental absorption spectra, we performed Time-Dependent Density Functional Theory calculations (TD-DFT) on solvated systems in their most stable spin state. To reproduce properly the range of experimental data, which covers a wavelength range from 700 to 200 nm, we included in TD-DFT computations 140 absorption transitions for cations derived from **1a** and **1b** compounds, and 250 transitions in the **1c** case. Within the well-accepted electric dipole approximation, the experimental measurements of absorbance are directly proportional to the oscillator strengths of transitions as determined by theory. We further processed rough theoretical data by broadening delta-like absorption peaks with a Gaussian function having a FWHM of 0.3 eV. Theoretical data have been fitted with the same criteria adopted for experimental ones. This procedure allows for an easier comparison between recorded and computed spectra. Computed absorption lines fall at somewhat higher energies with respect to experimental ones, which comes as no surprise. In the specific systems studied here, this effect corresponds to a shift of a few tens of nanometers, which does not prevent a direct comparison between experimental and theoretical sets of data. The overall good agreement between the experiment and theoretical simulations is a non-trivial argument in favor of the capability of our approach in characterizing these complexes.

Single crystal X-ray diffraction analysis of compound **1a'**

Single crystals of **1a'** suitable for X-ray diffraction were isolated by slow diffusion of diethyl ether, layered on top of a methanolic solution of compound **1a** (*v/v* 2:1). A dark brown, elongated plate-like crystal of **1a'** (0.380 x 0.089 x 0.066 mm^3) was mounted on a MiTeGen Microloop and measured at 150 K. Data were collected on a XtaLAB Synergy S diffractometer (Rigaku), equipped with Oxford Cryostream 1000 and a micro-focus sealed X-ray tube with copper radiation (Cu-Kα, λ = 1.54184 Å), with the generator working at 50 kV and 1 mA. Data collection, frame integration, and data reduction were carried out with CrysAlis Pro[7] version 1.171.42.54a, using an empirical absorption correction with spherical harmonics (SCALE3 ABSPACK). The structure was solved by dual space methods with SHELXT-2015[8] and refined by iterative cycles of full-matrix least-square routines against F2 with SHELXL-2018[8] within the WinGX program suite.[9] All non-hydrogen atoms were refined using anisotropic thermal parameters, while the hydrogen atoms were modelled on idealized positions with U_{iso} = 1.2 U_{eq}. The ORTEP molecular plots (50%) and structural representations were generated with DIAMOND[16] version 4.0.

Compound **1a'** crystallizes in the monoclinic space group *C*2/*m* (No. 12), as confirmed by systematic absences observed in the diffraction data. The formula unit contains two positively charged $[FeCl_2(Pc\text{-}L)]^+$ monomers, which are balanced by a $[FeCl_4]^{2-}$ counterion (Fig. S1a). The Fe(II) anion is highly disordered, which is reflected by a relatively high R(int) value on the collected data (10.2%), exhibiting a double tetrahedral geometry (Fig. S1b) with its atoms generated by symmetry. In the first few cycles of refinement, the Fe(II) center of the $[FeCl_4]^{2-}$ moiety occupied a crystallographic special position (coinciding with both a center of inversion and a 2-fold axis), resulting in positional disorder of the four coordinated chlorines. To accurately assess this disorder, the structural refinement was initially tested in the lower symmetry space group *Cm* (No. 18), derived from the initial space group by

removing the 2-fold axis and inversion center. This approach allows for independent treatment of the two opposite $[FeCl_4]^{2-}$ fragments with variable occupancy, confirming a near-equal probability (0.555:0.445) for the two orientations and indicating that the disorder does not lead to a total disruption of the average crystal symmetry.

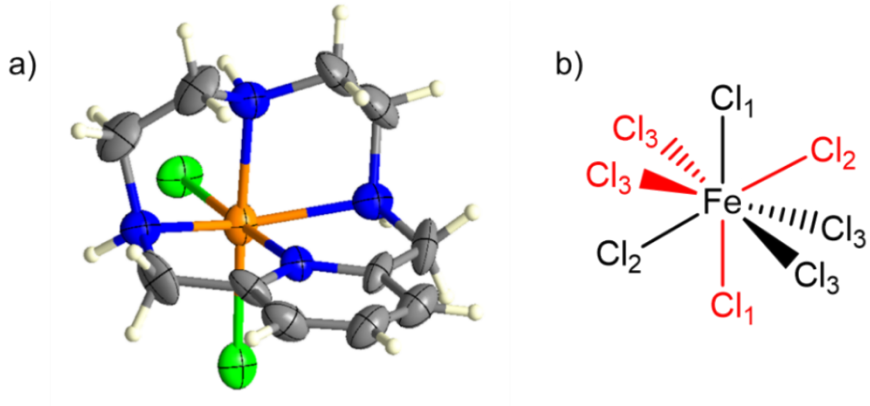

Figure S1. a) Molecular structure of the $[FeCl_2(Pc\text{-}L)]^+$ complex in **1a'**. Thermal ellipsoids are drawn at 50% probability. Colors: Fe, orange; Cl, green; N, blue; C, grey; H, white. b) Schematic representation of the symmetry-generated double tetrahedral geometry of the disordered $[FeCl_4]^{2-}$ counterion. Subscripts denote crystallographically equivalent chloride positions.

Based on this, the final refinement was performed in the higher symmetry space group *C*2/*m* (Table S1, Fig. S2) and allowing the Fe(II) center of the anion to be slightly displaced from the inversion center. This displacement results in the doubling of the Fe(II) site by symmetry, which is better able to account for the larger distribution of electron density in the unit cell caused by the disorder (R_1= 6.76%, wR_2 = 0.1715). The $[FeCl_4]^{2-}$ anion exhibits Fe-Cl bond distances between 1.93 – 2.42 Å and Cl-Fe-Cl angles between 108.8° – 110.8°, compared to the 2.13-2.44 Å and 101.1° - 122.4° ranges observed for entries in the Cambridge Structural Database containing the same species. The $[FeCl_2(Pc\text{-}L)]^+$ complex structure obtained in the high-symmetry *C*2/*m* space group is consistent with the observed features of the *Cm* model, although with lower standard uncertainties due to the reduced number of parameters. Table S2 and S3 list selected bond distances and angles, as well as potential intermolecular hydrogen bonds between the different moieties in the unit cell, as determined by PARST[17] calculations.

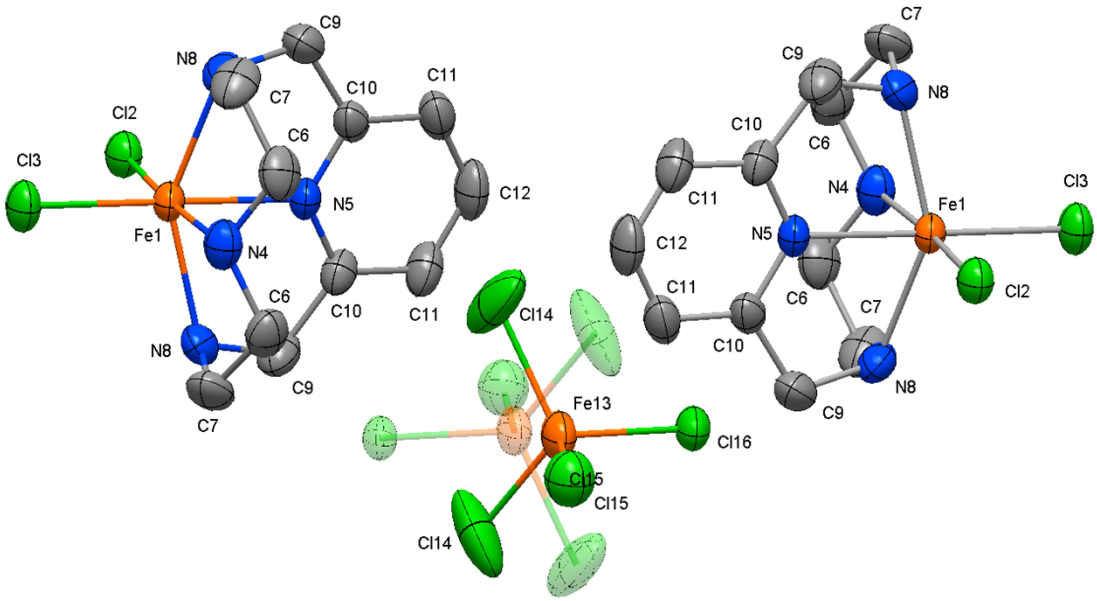

Figure S2. Representation of the crystal structure of **1a'** solved in the *C*2/*m* space group (No. 12), refined with anisotropic displacement parameters. Thermal ellipsoids are drawn at 50% probability. Disordered sites are depicted with lower opacity. Colors: Fe, orange; Cl, green; N, blue; C, grey; Hydrogen atoms are omitted for clarity.

Full crystallographic data have been deposited with the Cambridge Crystallographic Data Centre (CCDC No. 2404719) and can be obtained free of charge via www.ccdc.cam.ac.uk/data_request/cif, by emailing data_request@ccdc.cam.ac.uk, or by contacting The Cambridge Crystallographic Data Centre, 12 Union Road, Cambridge CB2 1EZ, UK; fax: +44 1223 336033.

Table S1. Summary of crystallographic data and refinement details for compound **1a'**.

CCDC No.	**2404719**
Formula	$C_{22}H_{36}Cl_8Fe_3N_8$
Formula weight	863.74
Crystal system	Monoclinic
Space group	*C*2/*m*
a [Å]	27.7537(10)
b [Å]	8.7587(4)
c [Å]	7.0757(3)
α [°]	90.00
β [°]	90.105(4)
γ [°]	90.00
V [Å^3]	1720.00(12)
Z	2
Radiation type	Cu-Kα (λ = 1.54184)
Temp. [K]	150(2)
$\rho_{(calcd)}$ [g·cm^{-3}]	1.668
μ [mm^{-1}]	15.966
F(000)	527.5
Cryst. size [mm^3]	0.38 x 0.09 x 0.07
θ range [°]	3.1847 – 80.6721
Limiting indices	-35<=h<=34; -8<=k<=10; -9<=l<=9
Reflections collected/unique[a]	15600 / 1977 [R(int) = 0.1024, R(σ) = 0.0473]
Data/restraints/parameters	1977 / 0 / 118
Completeness [%]	99.7
Final R indices (I > 2σ(I))[b]	R1 = 0.0676, wR2 = 0.1715
R indices (all data)	R1 = 0.0839, wR2 = 0.1914
Goodness of fit[c] on F^2	1.032
Largest diff. peak and hole [Å^{-3}]	0.92 and -0.63

[a] $R_{int} = \Sigma|F_o^2 - F_o^2(mean)|/\Sigma F_o^2$

[b] $R_1 = \Sigma||F_o| - |F_c||/\Sigma|F_o|$, $wR_2 = \{\Sigma[w(F_o^2 - F_c^2)^2]/\Sigma[w(F_o^2)^2]\}^{1/2}$

[c] $GooF = \{S/(n - p)\}^{1/2} = \{\Sigma[w(F_o^2 - F_c^2)^2]/(n - p)\}^{1/2}$.

Table S2. Selected bond distances and angles for **1a'** solved in the *Cm* space group, calculated using PARST.[17]

Atom Names	Distance / Å	Atom Names	Angle / °	Atom Names	Angle / °
Fe1 - Cl2	2.381(2)	Cl3 - Fe1 - Cl2	93.84(7)	C9 - N8 - Fe1[1]	111.4(3)
Fe1 - Cl3	2.3077(17)	N4 - Fe1 - Cl2	174.78(17)	C9 - N8 - C7	114.3(5)
Fe1 - N4	2.179(6)	N4 - Fe1 - Cl3	91.39(17)	C10 - C9 - N8	112.5(4)
Fe1 - N5	2.132(5)	N5 - Fe1 - Cl2	88.05(16)	C9 - C10 - N5[1]	116.2(4)
Fe1 - N8[1]	2.205(4)	N5 - Fe1 - Cl3	178.12(17)	C11 - C10 - N5[1]	120.1(5)
Fe1 - N8	2.205(4)	N5 - Fe1 - N4	86.7(2)	C11 - C10 - C9	123.7(5)
N4 - C6[1]	1.466(6)	N8[1] - Fe1 - Cl2	99.37(13)	C12[1] - C11 - C10	118.3(5)
N4 - C6	1.466(6)	N8 - Fe1 - Cl2	99.37(13)	C11 - C12 - C11[1]	121.2(7)
N5 - C10[1]	1.333(5)	N8[1] - Fe1 - Cl3	103.55(11)	Cl14[2] - Fe13 - Cl14	110.1(3)
N5 - C10	1.333(5)	N8 - Fe1 - Cl3	103.55(11)	Cl14[4] - Fe13 - Cl14[3]	136.8(4)
C6 - C7	1.512(8)	N8[1] - Fe1 - N4	79.37(13)	Cl15 - Fe13 - Cl14[2]	109.57(19)
C7 - N8	1.478(8)	N8 - Fe1 - N4	79.37(13)	Cl15[4] - Fe13 - Cl14[3]	110.8(2)
N8 - C9	1.478(7)	N8 - Fe1 - N5	76.11(11)	Cl15 - Fe13 - Cl14	109.57(19)
C9 - C10	1.498(8)	N81 - Fe1 - N5	76.11(11)	Cl15[4] - Fe13 - Cl14[4]	110.8(2)
C10 - C11	1.394(7)	N8 - Fe1 - N8[1]	145.7(2)	Cl16 - Fe13 - Cl14	108.80(15)
C11 - C12[1]	1.368(7)	C6 - N4 - Fe1	110.5(3)	Cl16 - Fe13 - Cl14[2]	108.80(15)
Fe13 - Fe13[2]	0.663(4)	C61 - N4 - Fe1	110.5(3)	Cl16 - Fe13 - Cl15	109.9(2)
Fe13 - Cl14[3]	1.931(5)	C6 - N4 - C6[1]	115.0(6)		
Fe13 - Cl14[4]	2.189(4)	C10[1] - N5 - Fe1	118.9(3)		
Fe13 - Cl14	2.189(4)	C10 - N5 - Fe1	118.9(3)		
Fe13 - Cl14[2]	1.931(5)	C10 - N5 - C10[1]	122.0(6)		
Fe13 - Cl15[2]	2.419(6)	C7 - C6 - N4[1]	108.1(4)		
Fe13 - Cl15	2.207(6)	N8 - C7 - C6	109.9(4)		
Fe13 - Cl16	2.187(4)	C7 - N8 - Fe1[1]	107.1(4)		

[1] +X,1-Y,+Z; [2] +X,2-Y,+Z; [3] 1-X,2-Y,-Z; [4] 1-X,+Y,-Z.

Table S3. Possible hydrogen bonds for **1a'** calculated using PARST.[17]

D-H···A	D···A Distance / Å	H···A Distance / Å	D-H-A Angle / °
N4-H4···Cl12	3.281(.006)	2.357(.002)	153.33(0.36)
C6-H6A···Cl14	3.487(.007)	2.728(.005)	133.78(0.32)
N8-H8···Cl12	3.386(.004)	2.494(.001)	148.31(0.24)
C9-H9B···Cl3	3.627(.006)	2.770(.001)	145.14(0.34)

Structural comparison between O_h-[$Fe^{III}X_2$(Pc-L)]$^+$ complexes

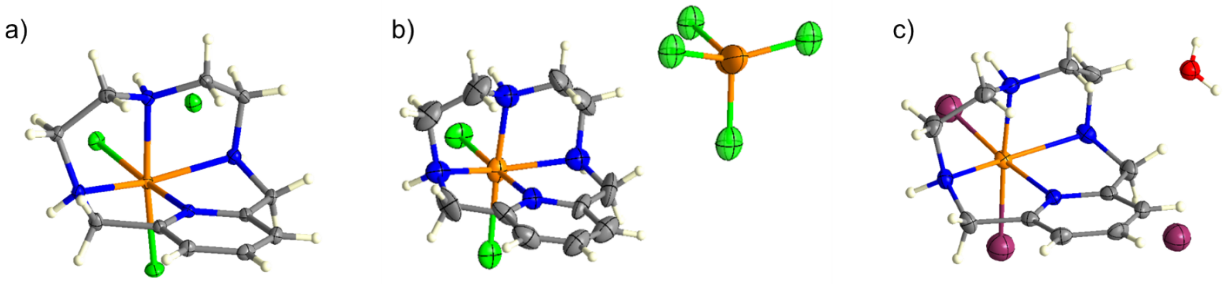

Figure S3. . X-ray diffraction molecular structure of complex a) **1a** (CCDC No 1578766), b) **1a′** (this work, CCDC No 2404719), and c) **1b** (CCDC No 2016034). Thermal ellipsoids are drawn at 50% probability. Colors: Fe, orange; Cl, green; N, blue; C, grey; Br, purple; H, white; O, red.

1a, **1a'**, and **1b** (Figures S3a-c) exhibit structural parameters and solid-state arrangements comparable to other reported O_h-[FeX_2(pyclen)]$^+$ complexes. The Fe(III) center adopts a distorted octahedral geometry, coordinated by the four nitrogen atoms of the macrocycle and by two monodentate X-type ligands. The pyclen scaffold displays a *cis*-folded conformation, which has been demonstrated by molecular mechanics calculations to be preferred when M–N bond lengths are greater than 2.0 Å.[19] The Fe(III) ion is slightly displaced from the tetraaza-macrocyclic cavity (d_{FeN4} = 1.085 - 1.112 Å), due to electronic and steric effects imposed by the ligand structure. Tables S4 and S5 present a comparison of relevant geometric parameters between the structures reported here and related ones found in the literature. The Fe–N(sp^2), Fe–N(sp^3), and Fe–X bond lengths fall within the expected ranges.

Experimental structures were compared with gas-phase and solvated **1a**, **1b**, and **1c** species as computed by theory. Although, in principle, the crystal field in solid-state systems is likely to affect the octahedral distortion around iron atoms, our analysis shows that the arrangement of the ligands can be primarily ascribed to the isolated complex itself, rather than to crystal packing. Experimental and theoretical data collected in Tables S4 and S5 allow to draw the following consistent picture: (a) the displacement of iron from the macrocyclic cavity ranges from 1.1 to 1.2 Å; (b) the two Fe–X bonds differ in length by a quite small amount, of the order of 10^{-2} Å; (c) the X–Fe–X angle spans a quite large range depending on the moiety and the phase, but it's always larger than the ideal value of 90°; (d) the Fe–N(sp^2) bond is always shorter than Fe–N(sp^3) one, and their difference measures about 0.1 Å; (e) the N_{ax}–Fe–N(sp^3) angle deviates from the ideal value of 90° by just 5°, while the N_{eq}–Fe–N_{eq} angle is smaller than 180° by the quite large amount of 35°. Overall, theoretical data obtained for cations derived from **1a**, **1b,** and **1c** nicely agree with experimental X-rays structure analysis.

Table S4. Comparison between the displacement of the iron(III) center from the macrocyclic cavity, Fe–X bond distance and X–Fe–X angles for O_h-$[FeX_2(pyclen)]^+$ complexes balanced with different counterions, as determined by the SC-XRD structures and DFT calculations. Theoretical data refers to the gas-phase (gas) and solvated (solv) anions in the high spin arrangement, which proved to be the most stable (*vide infra*).

Complex	dFeN4 (Å)	Fe–X (Å)	X–Fe–X (°)	Ref.
$[FeCl_2(pyclen)]Cl$	1.087	2.280 - 2.286	95.8	This work (**1a**), [17]
$[FeCl_2(pyclen)]^+_{gas}$	1.191	2.215 - 2.232	103.5	This work, theor.
$[FeCl_2(pyclen)]^+_{solv}$	1.142	2.300 - 2.303	97.6	This work, theor.
$[FeCl_2(pyclen)]_2[FeCl_4]$	1.109	2.295 - 2.389	93.8	This work (**1a'**)
$[FeBr_2(pyclen)]Br$	1.085	2.422 - 2.435	96.0	This work (**1b**), [4]
$[FeBr_2(pyclen)]^+_{gas}$	1.198	2.331 - 2.346	104.5	This work, theor.
$[FeBr_2(pyclen)]^+_{solv}$	1.162	2.386 - 2.390	100.5	This work, theor.
$[Fe(OTf)_2(pyclen)]^+_{gas}$	1.144	1.897 - 1.899	97.3	This work, theor.
$[Fe(OTf)_2(pyclen)]^+_{solv}$	1.103	1.952 - 2.005	91.0	This work, theor.
$[FeCl_2(pyclen)]BF_4$	1.092	2.257 - 2.283	98.8	[18]
$[FeCl_2(pyclen)]ClO_4$	1.093	2.264 - 2.282	99.3	[19]
$[\mu\text{-}O(pyclenFeCl)_2]_2ClO_4$	1.127	2.323 (Cl), 1.784 (μO)	93.7	[20]
$[FeCl_2(pyclen)]CF_3SO_4$	1.098	2.260 - 2.272	98.4	[21]
$[\mu\text{-}O(pyclenFeCl)_2]Cl,ClO_4$	1.126	2.329 (Cl), 1.778 ((μO)	99.5	[20]

Table S5. Comparison between bond distances and angles of the iron(III) center with the nitrogen atoms of the pyclen scaffold for O_h-$[FeX_2(pyclen)]^+$ complexes balanced with different counterions, as determined by the SC-XRD structures and DFT calculations. Theoretical data refers to the gas-phase (gas) and solvated (solv) anions in the high spin arrangement, which proved to be the most stable (*vide infra*).

Complex	Fe–N(sp^2) (Å)	Fe–N(sp^3) (Å)	N_{eq}–Fe–N_{eq} (°) [a]	N_{ax}–Fe–N(sp^2) (°) [b]	Ref.
$[FeCl_2(pyclen)]Cl$	2.098	2.161 - 2.182	146.7	86.6	This work (**1a**), [17]
$[FeCl_2(pyclen)]^+_{gas}$	2.155	2.231 - 2.303	142.7	82.3	This work, theor.
$[FeCl_2(pyclen)]^+_{solv}$	2.131	2.205 - 2.245	144.2	85.0	This work, theor.
$[FeCl_2(pyclen)]_2[FeCl_4]$	2.146	2.172 - 2.196	145.4	85.4	This work (**1a'**)
$[FeBr_2(pyclen)]Br$	2.102	2.169 - 2.188	147.6	85.6	This work (**1b**), [4]
$[FeBr_2(pyclen)]^+_{gas}$	2.158	2.232 - 2.313	142.4	82.0	This work, theor.
$[FeBr_2(pyclen)]^+_{solv}$	2.138	2.218 - 2.272	143.5	84.1	This work, theor.
$[Fe(OTf)_2(pyclen)]^+_{gas}$	2.133	2.270 - 2.340	146.4	84.8	This work, theor.
$[Fe(OTf)_2(pyclen)]^+_{solv}$	2.095	2.261 - 2.274	147.7	86.9	This work, theor.
$[FeCl_2(pyclen)]BF_4$	2.108	2.163 - 2.195	146.9	86.0	[18]
$[FeCl_2(pyclen)]ClO_4$	2.107	2.164 - 2.200	147.3	85.6	[19]
$[\mu\text{-}O(pyclenFeCl)_2]_2ClO_4$	2.133	2.153 - 2.575	144.7	85.4	[20]
$[FeCl_2(pyclen)]CF_3SO_4$	2.114	2.158 - 2.197	147.1	85.2	[21]
$[\mu\text{-}O(pyclenFeCl)_2]Cl,ClO_4$	2.136	2.137 - 2.218	145.6	84.3	[20]

[a] Angle between the equatorial N(sp^3) atoms; [b] angle between the axial N(sp^3) atom and the N(sp^2) of the pyridine moiety.

To comprehensively represent the molecular geometry and structural distortion in the octahedral coordination complexes, the following parameters have been determined for each $[FeX_2(Pc\text{-}L)]^+$ species reported as of now, including those presented in this work (Table S6 and S7). Overall, the structural descriptors of the present complexes are consistent with those of previously reported structures, suggesting similar spatial conformation and degree of Jahn-Teller distortion across the series.

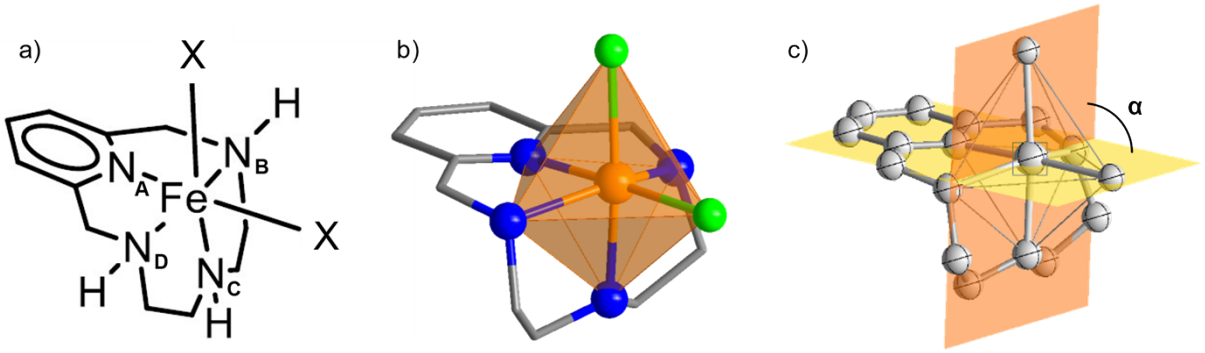

Figure S4. a) Schematic representation, b) octahedral coordination sphere, and c) Jahn-Teller distortion parameter **α** of complexes of general formula $[FeX_2(Pc\text{-}L)]^+$.

- Pc-L scaffold conformation,[18] that can be described by the positions of the N-H hydrogen atoms, designated as either above (+) or below (-) the N_4-coordination plane.
- Iron(III) center displacement[19] from the macrocyclic cavity, as expressed by its distance (d_{FeN4}) from the N_4 mean least-square plane.
- Folding angle (Ω),[19] which is a measure of the arrangement of the macrocyclic ring along the axis defined by the nitrogen atoms close to the pyridine ring and corresponds to the dihedral angle between the [N_A, N_B, N_D] and [N_B, N_C, N_D] planes illustrated in Fig. S4a.
- Degree of distortion[20] of the coordination sphere from an ideal octahedron (Fig. S4b), in terms of average Fe-L distances (d_{mean}), bond stretching (ζ), angular (Σ), and torsional (Θ) distortions.

$$\zeta = \sum_{i=1}^{6} |d_i - d_{mean}| \quad \Sigma = \sum_{i=1}^{12} |90 - \phi_i| \quad \Theta = \sum_{i=1}^{24} |60 - \theta_i|$$

  For reference, an ideal O_h-FeL_6 metal complex would be characterized by d_{mean} = 1.460 Å, ζ = 0.00 Å, and Σ = Θ = 0.00°.

- Angular Jahn-Teller distortion[21,22] parameter (α), defined as the dihedral angle between the mean least-square plane containing the equatorial and axial ligand (Fig. S4c). The larger the variation from 90°, the greater the magnitude of the Jahn-Teller effect on the octahedral geometry.

Table S6. Structural parameters for O_h-$[FeX_2(Pc\text{-}L)]^+$ complexes balanced with different counterions.

CCDC No.	X	Anion	Pc-L Conf.	d_{FeN4} (Å)	Ω (°)	α (°)	Ref.
1578766	Cl	Cl-	+++	1.087	65.30	87.97	This work (**1a**), [23]
2404719[a]	Cl	$[FeCl_4]^{2-}$	+++	1.109	63.95	87.67	This work (**1a'**)
2016034	Br	Br-	+++	1.085	67.36	83.78	This work (**1b**), [4]
639154	Cl	BF_4-	+++	1.092	66.63	87.11	[24]
1422489	Cl	ClO_4-	+++	1.093	67.44	87.83	[25]
1578765[b]	Cl μ_2O	ClO_4-	+++	1.127	65.06	87.67	[26]
1977733	Cl	CF_3SO_4-	+++	1.098	67.85	88.02	[27]
2018374[c]	Cl μ_2O	ClO_4-, Cl-	+++	1.126	67.42	86.18	[26]

[a] The values reported are averaged between the two monomers contained in the asymmetric unit; [b] Dimeric complex with symmetrically equivalent monomers; [c] Dimeric complex with asymmetric monomers; here the averaged values are reported.

Table S7. Octahedral distortion parameters for O_h-$[FeX_2(Pc\text{-}L)]^+$ complexes balanced with different counterions.

CCDC No.	X	Anion	d_{mean} (Å)	ζ (Å)	Σ (°)	Θ (°)	Ref.
1578766	Cl	Cl-	2.198	0.340	106.49	285.49	This work (**1a**), [23]
2404719[a]	Cl	$[FeCl_4]^{2-}$	2.232	0.443	105.72	284.40	This work (**1a'**)
2016034	Br	Br-	2.250	0.716	101.21	267.56	This work (**1b**), [4]
639154	Cl	BF_4-	2.195	0.300	107.75	266.80	[24]
1422489	Cl	ClO_4-	2.198	0.307	107.74	266.07	[25]
1578765[b]	Cl μ_2O	ClO_4-	2.139	0.722	108.39	276.59	[26]
1977733	Cl	CF_3SO_4-	2.196	0.280	106.85	264.26	[27]
2018374[c]	Cl μ_2O	ClO_4-, Cl-	2.142	0.738	112.76	277.49	[26]

[a] The values reported are averaged between the two monomers contained in the asymmetric unit; [b] Dimeric complex with symmetrically equivalent monomers; [c] Dimeric complex with asymmetric monomers; here the averaged values are reported.

Mössbauer spectrum of commercial $Fe(OTf)_3$

Table S8. Results of the Mössbauer refinement for the spectra of **1a-c** and commercial $Fe(OTf)_3$. S corresponds to the spin, δ is the isomer shift, ΔE_Q is the quadrupole splitting, w is the mass percentage of the corresponding iron state.

Sample	Oxidation state	S	$\delta\ (mm/s)$	$\Delta E_Q\ (mm/s)$	w (%)
1a	Fe^{3+} (oct.)	5/2	0.31	0.51	100
1b	Fe^{3+} (oct.)	5/2	0.32	0.39	81(2)
	Fe^{2+} (oct.)	2	0.98	1.95	19(3)
1c[a]	Fe^{3+} (oct.)	5/2	0.23	0.29	64(1)
	Fe^{2+} (oct.)	2	1.27	3.17	31(1)
	Fe^{2+} (impurity)	0	0.32	2.01	5(1)
1c[b]	Fe^{3+}	5/2	0.32	-	15(6)
	Fe^{3+}	5/2	0.49	-	85(4)

[a]Synthesized from commercially available $Fe(OTf)_3$. [b]Prepared starting from in-house synthesized $Fe(OTf)_3$ as the iron source.

The spectrum of sample **1a** (Figure S5, left) is relatively simple, consisting of a single doublet. This signal, characterized by an isomer shift (δ) of 0.31 mm/s and a quadrupole splitting (ΔE_q) of 0.51 mm/s, is unambiguously assigned to a high-spin Fe^{3+} species. A more complex situation is found in the case of sample **1b** (Figure S5, right). To achieve an optimal fit, the spectrum was deconvoluted into two subspectra. The primary component (≥ 80%) exhibits an isomer shift of 0.32 mm/s and a quadrupole splitting of 0.39 mm/s, consistent with a high-spin Fe^{3+} species. A minor subspectrum (≤ 20%) with an isomer shift of 0.98 mm/s and a quadrupole splitting of 1.95 mm/s indicates the presence of an iron(II) high-spin impurity, likely resulting from partial reduction of the starting material. The presence of Fe^{2+} was more evident in sample **1c** (Figure S6, left), which exhibited three subspectra, one of which corresponds to an iron(II) high spin species, contributing 32(2)% by weight. Unlike $FeBr_3$, which can easily reduce to $FeBr_2$ under vacuum and heating by evolving bromine, $Fe(OTf)_3$ is not expected to undergo a similar reaction. To confirm this, the commercial $Fe(OTf)_3$ starting material was analyzed using Mössbauer spectroscopy and found to contain up to 46% Fe^{2+} contamination (Table S9). Using the pure $Fe(OTf)_3$ source prepared in-house, sample **1c** did not show any evident sign of the presence of Fe^{2+} (Figure S6, right). However, the material's extreme hygroscopicity posed challenges during analysis. Exposure to atmospheric moisture likely led to ligand exchange, replacing triflate ligands with aquo ligands, producing a broad and poorly resolved spectrum. This spectrum was fitted with two broad singlets, but the low resolution precluded reliable quantitative analysis.

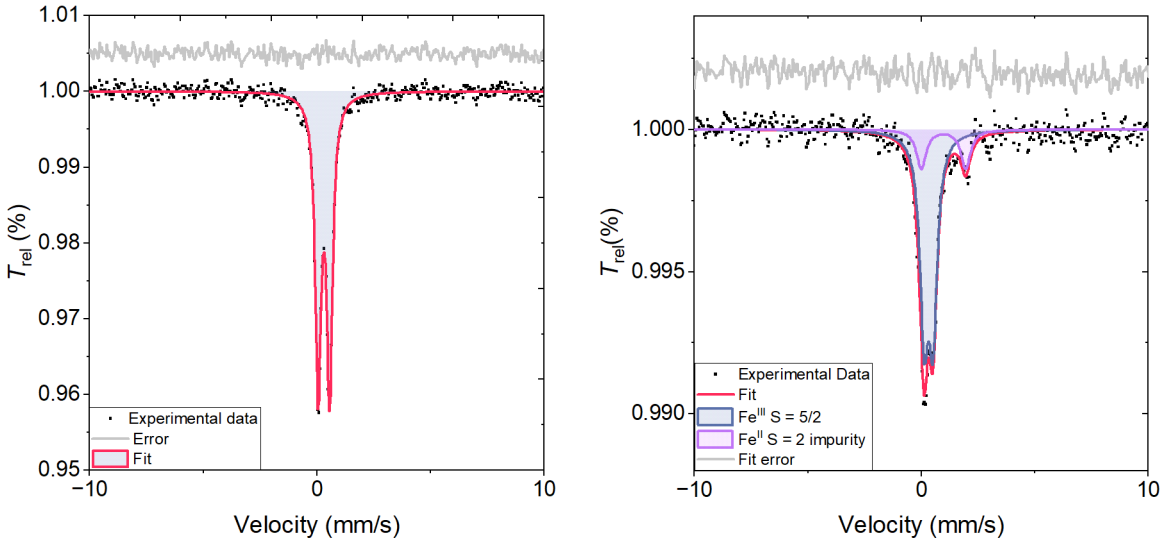

Figure S5. Mössbauer spectrum of compound **1a** (left) and **1b** (right).

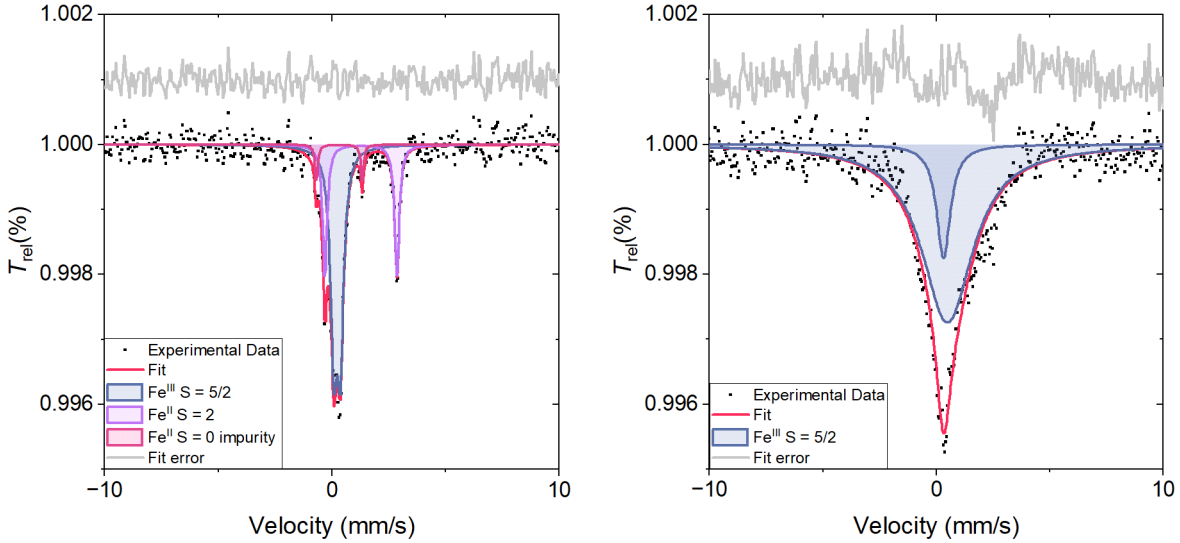

Figure S6. Mössbauer spectrum of compound **1c** prepared with commercial $Fe(OTf)_3$ as the iron source (left) and with in-house prepared $Fe(OTf)_3$ (right).

Table S9. *Mössbauer spectrum of commercial Fe(OTf)$_3$*

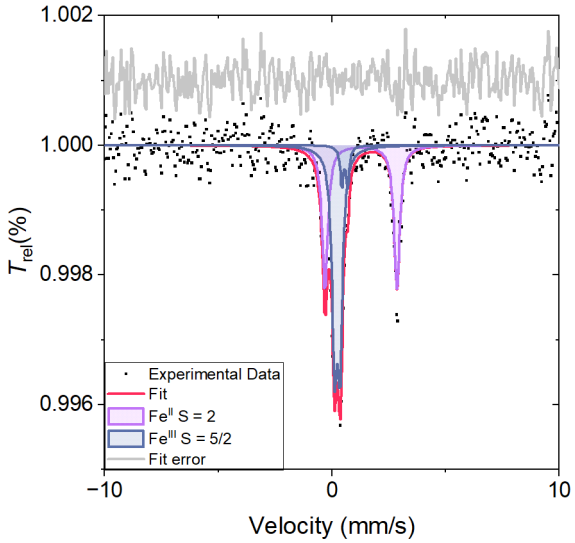

Sample	**Oxidation state**	S	$\delta\ (mm/s)$	$\Delta E_Q\ (mm/s)$	w (%)
Commercial Fe(OTf)$_3$	Fe^{3+} (oct.)	5/2	0.23	0.24	51(4)
	Fe^{2+} (oct.)	2	1.28	3.17	42(4)
	Impurity	-	0.56	0.26	6(3)

In Table S9 the Mössbauer spectrum of commercial Fe(OTf)$_3$ is reported along with the data from the fit.

Macroscopic magnetization measurements

Macroscopic magnetization measurements were conducted to further characterize the spin states of compounds **1a** and **1b**. A Quantum Design PPMS equipped with a VSM module was used to record Zero-Field-Cooled (ZFC) and Field-Cooled (FC) magnetic curves under an applied field of 0.5 T. In both cases, ZFC and FC curves overlapped, indicating the absence of magnetic irreversibility. For clarity, only the ZFC curves are presented here.

The temperature dependence of the molar magnetic susceptibility (χ_M) for compounds **1a** and **1b** is shown in Figure S7 and Figure S8, respectively. For compound **1a**, initial analysis using the **Curie law** yielded an effective magnetic moment (μ_{eff}) of 5.5164(4) μ_B, but clear deviations from ideal paramagnetic behavior were observed at lower temperatures. A subsequent Curie–Weiss law fit revealed antiferromagnetic interactions, with a Weiss constant (ϑ) of −5.28 K and a μ_{eff} of 5.7063(7) μ_B. Unfortunately, neither the Curie nor the Curie–Weiss models provided a satisfactory description of the data across the entire temperature range. In systems with an odd number of electrons, such as Fe^{3+} (d^5), the spin multiplicity is even, and the degeneracy cannot be completely lifted in zero field, resulting in zero-field splitting. This effect is well described in O. Kahn's *Molecular Magnetism*,[28] from which the Van Vleck formalism was adapted to model the magnetic behavior of compound **1a**, considering axial distortion and zero field splitting.

The magnetic susceptibility was expressed as:

$$\chi = \frac{\chi_z + 2\chi_x}{3}$$

$$\chi_z = \frac{Ng_z^2\mu_B^2}{4k(T-\theta)} \cdot \frac{1 + 9e^{-\frac{2D}{k(T-\theta)}} + 25e^{\frac{-6D}{k(T-\theta)}}}{1 + e^{-\frac{2D}{k(T-\theta)}} + e^{-\frac{6D}{k(T-\theta)}}}$$

$$\chi_x = \frac{Ng_x^2\mu_B^2}{4} \cdot \frac{\frac{9}{k(T-\theta)} + \frac{8}{D} - \frac{11e^{-\frac{2D}{k(T-\theta)}}}{2D} - \frac{5e^{-\frac{6D}{k(T-\theta)}}}{2D}}{1 + e^{-\frac{2D}{k(T-\theta)}} + e^{-\frac{6D}{k(T-\theta)}}}$$

Here, χ, χ_x, χ_z represent the global magnetic susceptibility and the magnetic susceptibility on the x and the z axis, respectively. N is Avogadro's number, g is the value of the g-tensor, μ_B is the Bohr's magneton, k is Boltzmann's constant, D is a value D-tensor such that $D = \frac{3D_{zz}}{2}$ (this formula considers only axial distortion), and T is the temperature. θ is an arbitrary temperature parameter accounting for antiferromagnetic interactions at lower temperatures.

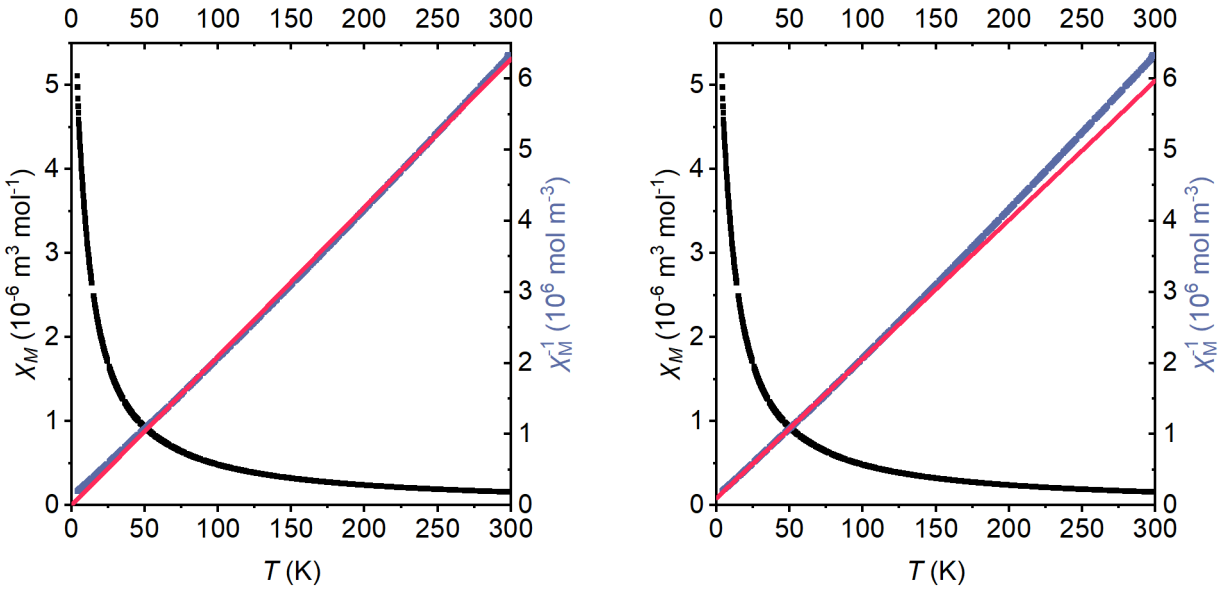

Figure S7. Curie and Curie-Weiss law fits of **1a**.

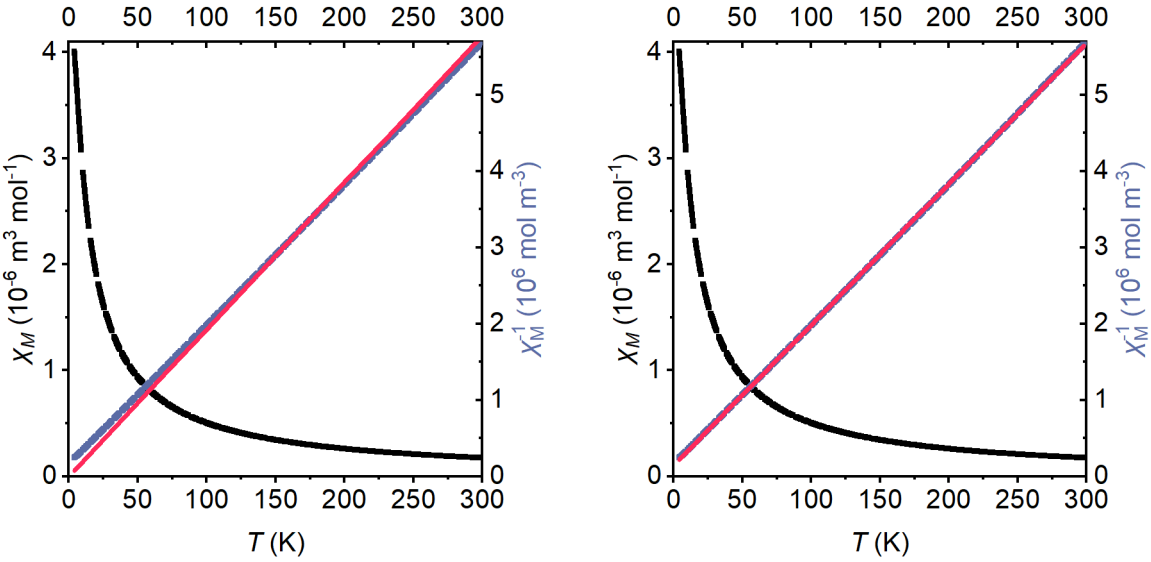

Figure S8. Curie and Curie-Weiss law fits of **1b**.

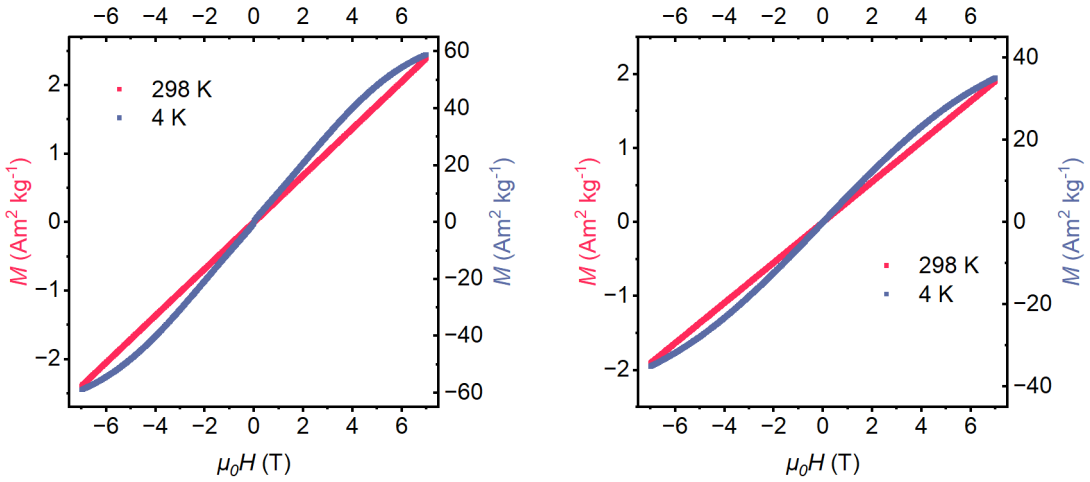

Figure S9. *Magnetization curve for **1a** (left) and **1b** (right).*

Isothermal magnetisation curves at room temperature show linear dependence of the magnetization characteristic for paramagnetic state (Figure S9). After cooling down to 4 K, the magnetisation curves do not show any visible hysteresis arising from the magnetic interactions. Regarding compound **1a**, a small deviation from the Brillouin function can be noticed at low magnetic fields (-0.025 T to 0.025 T). This could be due to the presence of small impurities giving rise to a different signal.

DFT calculation on the spin state of compounds **1a**, **1b** and **1c**: summary of the results

Table S10. *Relative stability of different spin states in **1a**, **1b** and **1c**. The most stable spin state of each compound and phase (gas, solvated) has been set to zero. All data include zero-point correction. Here **1a**, **1b** and **1c** refer to the anions extracted from the corresponding neutral compounds.*

Sample	Spin state	Energy, gas (kcal/mole)	Energy, solv. (kcal/mole)
1a	5/2	0	0
1a	3/2	+13.2	+13.6
1a	1/2	+14.1	+11.7
1b	5/2	0	0
1b	3/2	+10.8	+10.6
1b	1/2	+12.0	+9.7
1c	5/2	0	0
1c	3/2	+14.2	+17.2
1c	1/2	+27.6	+20.4

Spectroscopic characterization

In Figure S10, the experimental and simulated spectra of compounds **1a-c** are displayed. Herein, for completeness, all the Gaussians that were used for the fit are displayed.

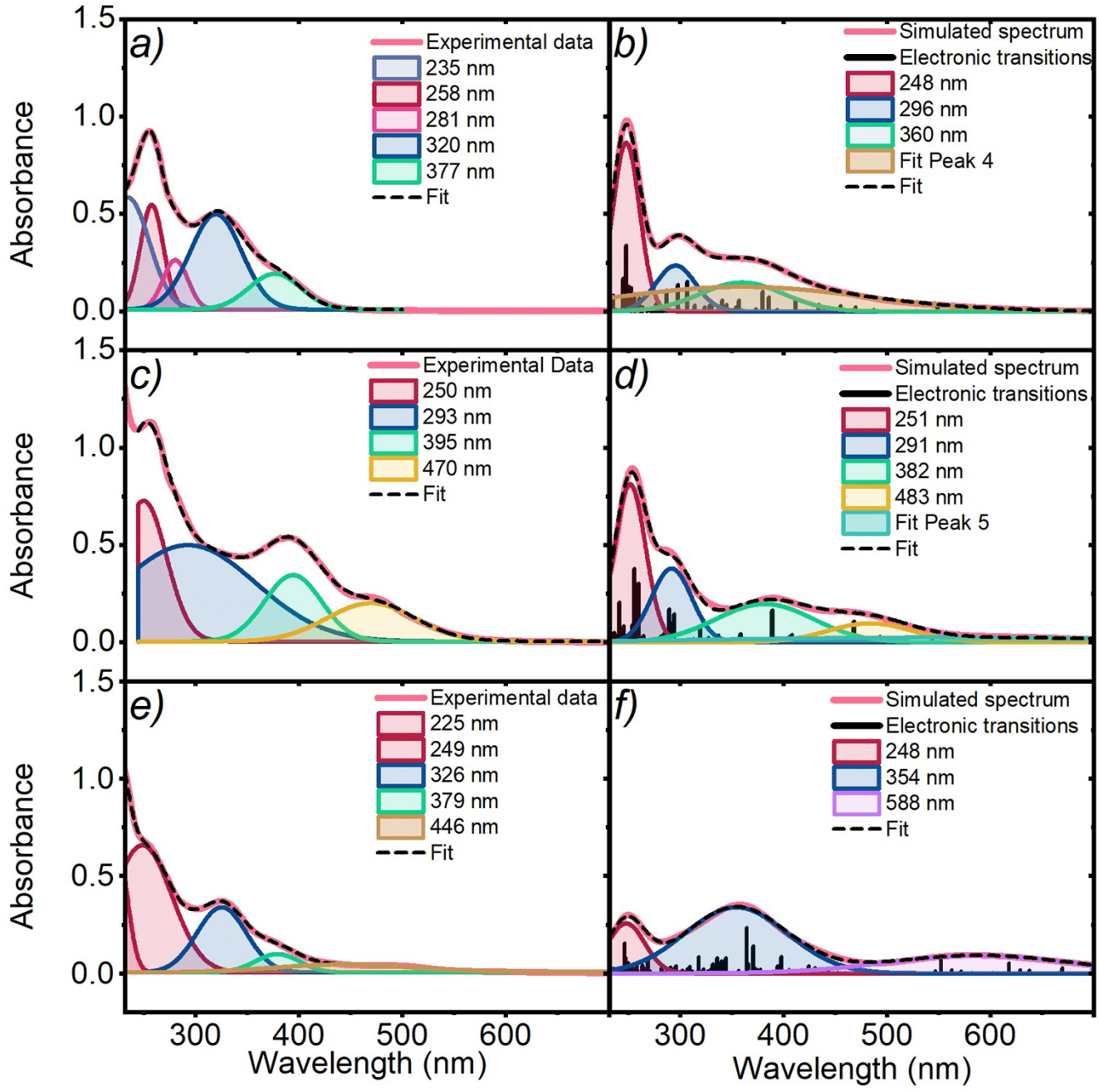

Figure S10. UV-vis experimental (left) and theoretical (right) spectra for **1a** (top) (a and b, respectively), **1b** (middle) (c and d), and **1c** (bottom) (e and f) complexes. Unlike Figure 3 in the manuscript, these plots display all the Gaussian curves that were used to fit the experimental data are displayed.

Photocatalytic tests

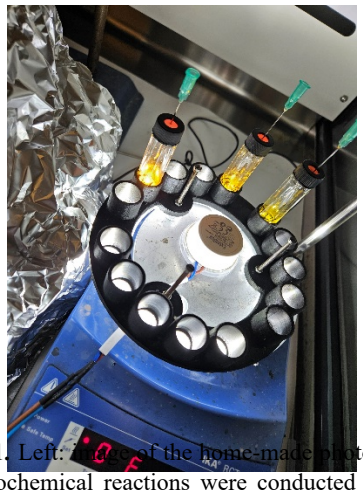

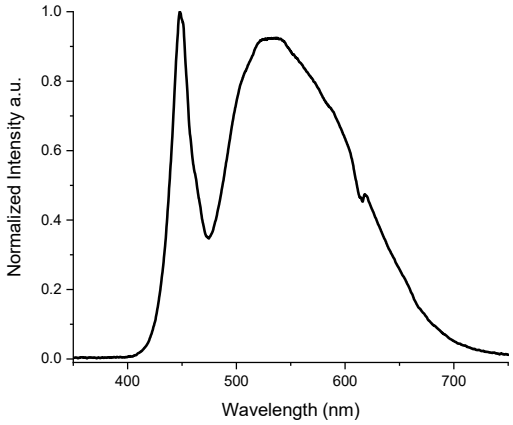

Figure S11. Left: picture of the home-made photoreactor. Right: emission spectra of the white lamp (33 mWcm^{-2}) used for photocatalytic tests. Photochemical reactions were conducted in 8 mL commercially available glass vials, with 1 ml solution (80 mM *p*-xylene in acetonitrile, 2.5 mM Fe pyclen derivatives, under air atmosphere).

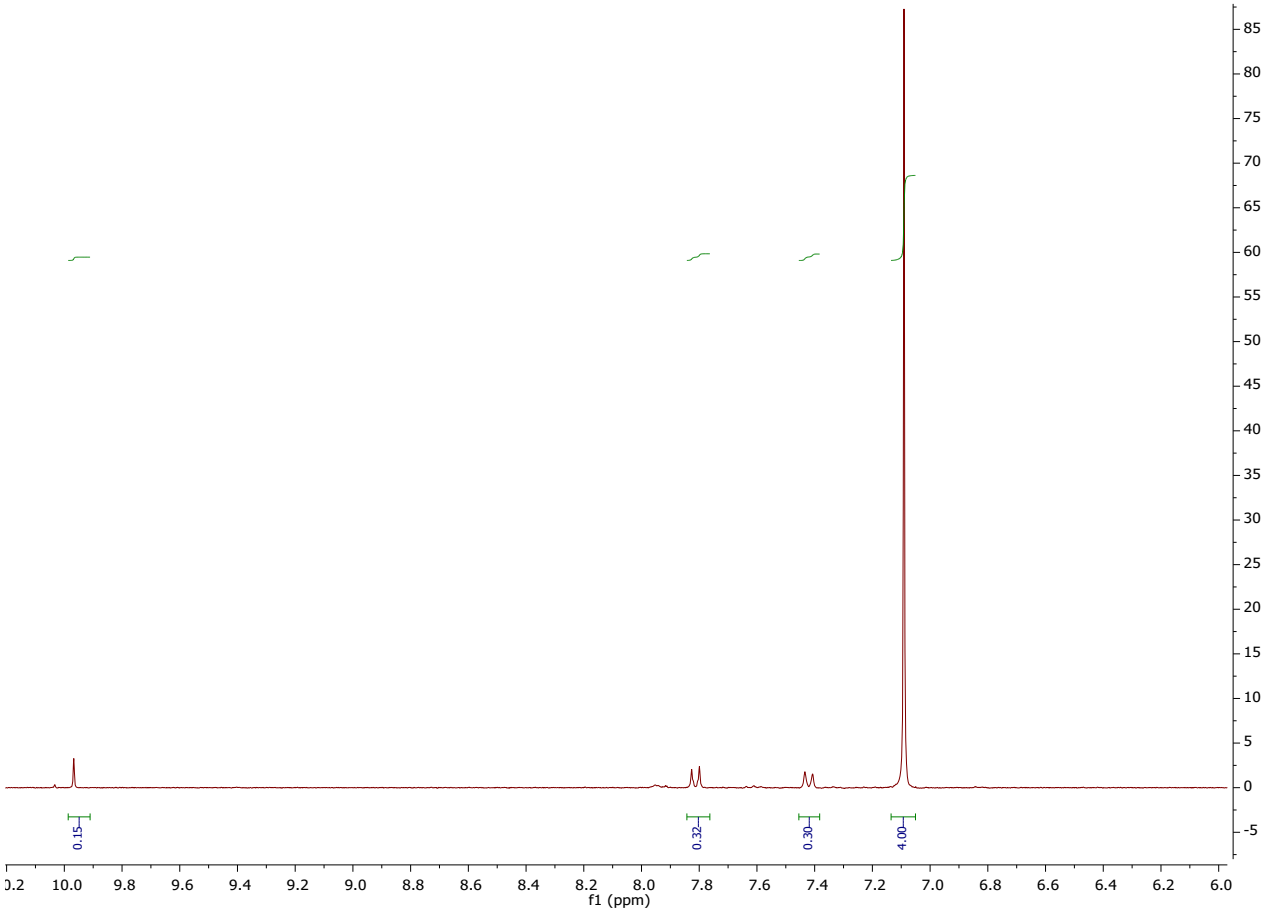

Figure S12. Representative ^{1}H NMR spectrum of the photocatalytic oxidation of *p*-xylene using Fe(pyclen)-Br **1b**. Standard conditions: 1 ml of solution containing 80 mM *p*-xylene and 2.5 mM Fe(pyclen)-Br **1b** in acetonitrile, irradiation with white light for 24 h under air atmosphere, according to Table 6. **^{1}H NMR** (300 MHz, CH_3CN /CD_3CN) δ 7,09 (s, 4H, aromatic protons of *p*-xylene), 7,42 and 7,81 (dd, J = 12, 6 Hz, 2 + 2 H, aromatic protons of the benzene ring in *p*-tolualdehyde), 9,97 (s, 1H, aldehydic proton of *p*-tolualdehyde).

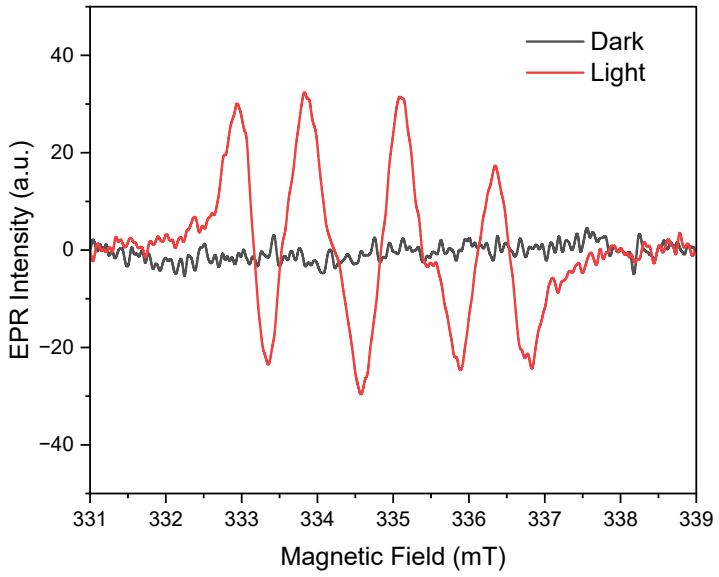

Figure S13. EPR spectra of a solution *p*-xylene (80 mM) and 2.5 mM **1b** in acetonitrile in the presence of BMPO, before and after irradiation with 405 nm LED.

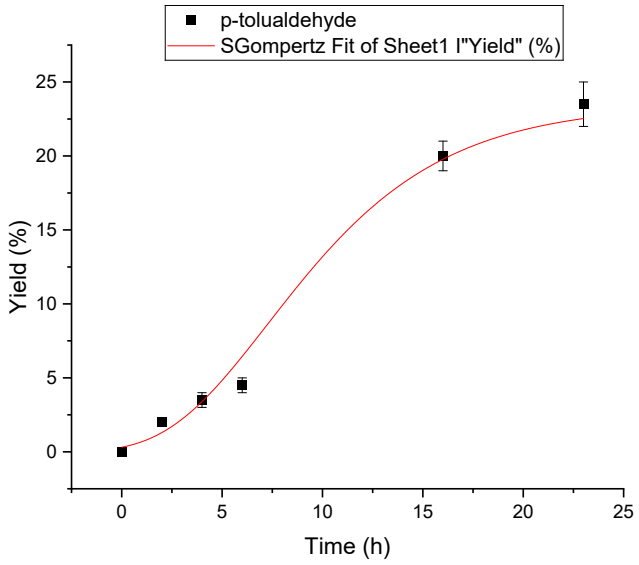

Figure S14. Kinetic profile of *p*-tolualdehyde production in the photochemical oxidation of *p*-xylene with white light in the presence of **1b**.

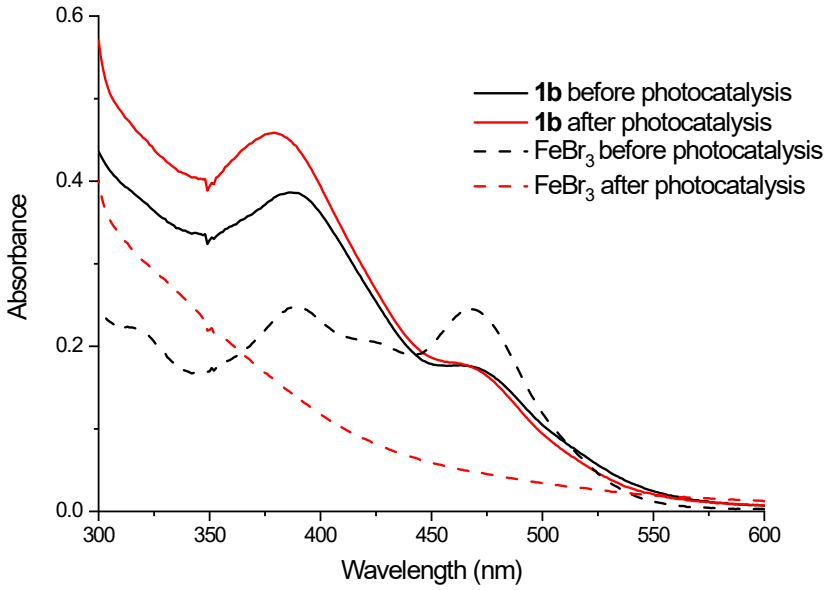

Figure S15. Uv-Vis spectra of Fe(pyclen)-Br **1b** (solid lines) and of $FeBr_3$ (dashed lines) before and after photocatalysis with white light (2.5 mM in acetonitrile, 80 mM *p*-xylene, 24 h irradiation under air atmosphere, 33 $mWcm^{-2}$).

Energies, spin, DFT functionals and basis set

(energies in kcal/mol)

1a

Functional	OPBE
Basis set	6-31G(d,p)
Calculation	Gas phase / opt
spin	Energy
5/2	0.0
3/2	13.1
1/2	13.2
Functional	OPBE
Basis set	6-31G(d,p)
Calculation	solvent / opt
spin	Energy
5/2	0.0
3/2	13.2
1/2	10.2
Functional	OPBE
Basis set	6-31G(d,p)
Calculation	Gas phase / opt + ZPE
spin	Energy
5/2	0.0
3/2	13.2
1/2	14.1
Functional	OPBE
Basis set	6-31G(d,p)
Calculation	solvent / opt + ZPE
spin	Energy
5/2	0.0
3/2	13.6
1/2	11.7
Functional	OPBE

Basis set	cc-pVTZ
Calculation	Gas phase / opt
spin	Energy
5/2	0.0
3/2	10.3
1/2	9.5
Functional	OPBE
Basis set	cc-pVTZ
Calculation	solvent / opt
spin	Energy
5/2	0.0
3/2	9.7
1/2	6.1
Functional	OPBE
Basis set	cc-pVTZ
Calculation	Gas phase / opt + ZPE
spin	Energy
5/2	0.0
3/2	10.5
1/2	10.5
Functional	OPBE
Basis set	cc-pVTZ
Calculation	solvent / opt + ZPE
spin	Energy
5/2	0.0
3/2	9.9
1/2	7.4
Functional	**ω**B97X
Basis set	cc-pVTZ
Calculation	Gas phase / geom(OPBE)
spin	Energy
5/2	0.0
3/2	11.5
1/2	13.4
Functional	**ω**B97X

Basis set	cc-pVTZ
Calculation	Gas phase / opt
spin	Energy
5/2	0.0
3/2	11.5
1/2	12.2

1b

Functional	OPBE
Basis set	6-31G(d,p)
Calculation	Gas phase / opt
spin	Energy
5/2	0.0
3/2	10.5
1/2	11.1
Functional	**ω**B97X
Basis set	cc-pVTZ
Calculation	Gas phase / geom(OPBE)
spin	Energy
5/2	0.0
3/2	10.6
1/2	14.4
Functional	**ω**B97X
Basis set	cc-pVTZ
Calculation	Gas phase / opt
spin	Energy
5/2	0.0
3/2	9.4
1/2	11.4

1c

Functional	OPBE
Basis set	6-31G(d,p)
Calculation	Gas phase / opt
spin	Energy
5/2	0.0
3/2	13.9
1/2	26.0
Functional	**ω**B97X
Basis set	cc-pVTZ
Calculation	Gas phase / geom(OPBE)
spin	Energy
5/2	0.0
3/2	11.1
1/2	17.2
Functional	**ω**B97X
Basis set	cc-pVTZ
Calculation	Gas phase / opt
spin	Energy
5/2	0.0
3/2	11.7
1/2	16.8

Spectral analysis of **1a**

Homolytic Fe-Cl bond breaking: 3.34 eV (371 nm). For each transition, we report the wavelength, the nature of the orbitals involved (number and nature, based on a visual inspection), their relative weight, and the oscillator strength. Data are taken from the solvated system. A=minority spin orbitals; B=majority spin orbitals.

Wavelength (nm)	Lower state	Upper state	weight	Oscillator strength
367.80	74B (pyclen)	84B (Fe)	0.59759	0.0000
	75B (Cl + pyclen)	84B (Fe)	0.68766	
	76B (pyclen)	84B (Fe)	0.34928	
	80B (Cl)	87B (Fe)	-0.14854	
362.07	74B (pyclen)	84B (Fe)	-0.66726	0.0005
	75B (Cl + pyclen)	84B (Fe)	0.69850	
	76B (pyclen)	84B (Fe)	-0.18136	
	80B (Cl)	87B (Fe)	0.12582	
359.51	75B (Cl + pyclen)	85B (Fe)	0.26457	0.0013
	76B (pyclen)	85B (Fe)	0.90410	
	78B (Cl + pyclen)	85B (Fe)	0.11237	
	79B (Cl)	86B (Fe)	0.19189	
	83B (Cl)	88B (Fe)	-0.14700	
357.03	76B (pyclen)	85B (Fe)	0.17588	0.0169
	77B (pyclen)	86B (Fe)	0.10275	
	81B (Cl + pyclen)	87B (Fe)	0.20244	
	83B (Cl)	88B (Fe)	0.94363	
354.25	74B (pyclen)	86B (Fe)	-0.15422	0.0069
	75B (Cl + pyclen)	84B (Fe)	-0.11385	
	76B (pyclen)	86B (Fe)	0.96333	
344.97	73B (Fe + Cl)	85B (Fe)	0.15738	0.0103
	73B (Fe + Cl)	88B (Fe)	0.13601	
	74B (pyclen)	85B (Fe)	0.20647	
	75B (Cl + pyclen)	85B (Fe)	0.88612	
	76B (pyclen)	85B (Fe)	-0.13441	
	78B (Cl + pyclen)	85B (Fe)	-0.12389	
	79B (Cl)	86B (Fe)	-0.20241	
343.93	73B (Fe + Cl)	84B (Fe)	-0.20438	0.0002
	74B (pyclen)	86B (Fe)	0.12135	
	82B (pyclen)	88B (Fe)	0.96412	
342.04	73B (Fe + Cl)	84B (Fe)	0.66817	0.0049
	74B (pyclen)	86B (Fe)	-0.36793	
	75B (Cl + pyclen)	86B (Fe)	-0.34791	
	76B (pyclen)	86B (Fe)	-0.18635	
	79B (Cl)	87B (Fe)	-0.15981	
	80B (Cl)	87B (Fe)	-0.37176	
	80B (Cl)	88B (Fe)	-0.11019	
	82B (pyclen)	88B (Fe)	0.24388	
340.93	87A (Fe + pyclen)	89A (pyclen)	-0.18576	0.0169
	77B (pyclen)	86B (Fe)	-0.11608	
	81B (Cl + pyclen)	87B (Fe)	0.92243	
	81B (Cl + pyclen)	88B (Fe)	-0.19150	
	83B (Cl)	88B (Fe)	-0.16394	
339.94	73B (Fe + Cl)	84B (Fe)	0.42210	0.0004
	75B (Cl + pyclen)	86B (Fe)	0.89140	

Spectral analysis of **1b**

Homolytic Fe-Br bond breaking: 2.94 eV (421 nm). For each transition, we report the wavelength, the nature of the orbitals involved (number and nature, based on a visual inspection), their relative weight, and the oscillator strength. Data are taken from the solvated system. A=alpha orbitals; B=beta orbitals.

Wavelength (nm)	Lower state	Upper state	weight	Oscillator strength
416.14	94B (Br)	102B (Fe)	0.11519	0.0000
	96B (Br + pyclen)	104B (Fe)	0.98065	
408.40	106A (Fe + pyclen)	107A (pyclen)	0.14009	0.0117
	93B (Fe + Br)	103B (Fe)	0.10166	
	95B (pyclen)	102B (Fe)	0.73164	
	96B (Br + pyclen)	103B (Fe)	-0.34359	
	97B (Br)	102B (Fe)	-0.12489	
	97B (Br)	104B (Fe)	0.29852	
	99B (Br + pyclen)	103B (Fe)	0.18946	
	100B (Br)	102B (Fe)	0.15165	
	101B (Br)	106B (Fe)	0.32927	
405.94	106A (Fe + pyclen)	107A (pyclen)	-0.37452	0.0088
	93B (Fe + Br)	103B (Fe)	-0.10652	
	95B (pyclen)	102B (Fe)	0.64328	
	96B (Br + pyclen)	103B (Fe)	0.27188	
	97B (Br)	104B (Fe)	-0.30011	
	99B (Br + pyclen)	103B (Fe)	-0.21648	
	100B (Br)	102B (Fe)	-0.17443	
	101B (Br)	106B (Fe)	-0.36301	
401.85	106A (Fe + pyclen)	107A (pyclen)	0.90124	0.0034
	95B (pyclen)	102B (Fe)	0.13774	
	96B (Br + pyclen)	103B (Fe)	0.13972	
	97B (Br)	104B (Fe)	-0.13130	
	101B (Br)	106B (Fe)	-0.31201	
389.42	106A (Fe + pyclen)	107A (pyclen)	0.11494	0.0489
	94B (Br)	106B (Fe)	-0.11677	
	96B (Br + pyclen)	103B (Fe)	0.28606	
	97B (Br)	104B (Fe)	-0.29762	
	99B (Br + pyclen)	103B (Fe)	-0.22600	
	99B (Br + pyclen)	105B (Fe)	0.11035	
	100B (Br)	102B (Fe)	-0.19158	
	101B (Br)	106B (Fe)	0.80604	
388.30	93B (Fe + Br)	102B (Fe)	0.28211	0.0000
	94B (Br)	102B (Fe)	-0.62600	
	95B (pyclen)	103B (Fe)	0.64463	
	96B (Br + pyclen)	104B (Fe)	0.13258	
	100B (Br)	105B (Fe)	0.24175	
386.61	91B (Fe + pyclen)	102B (Fe)	0.14662	0.0000
	93B (Fe + Br)	102B (Fe)	-0.19927	
	93B (Fe + Br)	104B (Fe)	-0.10855	
	94B (Br)	102B (Fe)	0.48023	
	95B (pyclen)	103B (Fe)	0.74007	
	96B (Br + pyclen)	104B (Fe)	-0.10022	
	100B (Br)	105B (Fe)	-0.35482	
382.45	91B (Fe + pyclen)	102B (Fe)	-0.22016	0.0001
	93B (Fe + Br)	102B (Fe)	0.46268	
	94B (Br)	102B (Fe)	0.57408	
	94B (Br)	104B (Fe)	-0.14034	

	100B (Br)	105B (Fe)	0.59195	
373.95	93B (Fe + Br)	103B (Fe)	0.27812	0.0006
	94B (Br)	103B (Fe)	-0.45365	
	95B (pyclen)	104B (Fe)	0.78320	
	99B (Br + pyclen)	105B (Fe)	0.25930	
369.72	92B (Fe + Br + pyclen)	103B (Fe)	-0.20098	0.0013
	94B (Br)	103B (Fe)	0.81862	
	95B (pyclen)	104B (Fe)	0.42484	
	96B (Br + pyclen)	103B (Fe)	-0.10247	
	99B (Br + pyclen)	105B (Fe)	0.23195	

Spectral analysis of **1c**

Homolytic Fe-Trif bond breaking: 3.89 eV (319 nm). This was estimated from the energy for homolytic Fe-Cl cleavage in **1a** (3.34 eV), summing the difference of BDFE in H-Tf and H-Cl at CISD level (0.55 eV). For each transition we report the wavelength, the nature of the orbitals involved (number and nature, based on a visual inspection), their relative weight and the oscillator strength. Data are taken from the solvated system. A=alpha orbitals; B=beta orbitals.

Wavelength (nm)	Lower state	Upper state	weight	Oscillator strength
499.71	142B (trif)	152B (Fe)	-0.12530	0.0001
	145B (trif)	152B (Fe)	0.21212	
	145B (trif)	153B (Fe)	-0.15855	
	146B (trif)	152B (Fe)	-0.45914	
	146B (trif)	153B (Fe)	0.10853	
	147B (pyclen)	154B (Fe)	0.77410	
	148B (pyclen)	155B (Fe)	0.10929	
494.30	143B (trif)	152B (Fe)	0.11535	0.0003
	145B (trif)	152B (Fe)	-0.43467	
	145B (trif)	153B (Fe)	-0.15173	
	146B (trif)	152B (Fe)	0.68625	
	146B (trif)	153B (Fe)	0.20026	
	147B (pyclen)	154B (Fe)	0.43512	
493.24	145B (trif)	152B (Fe)	0.81655	0.0013
	146B (trif)	152B (Fe)	0.53193	
	148B (pyclen)	152B (Fe)	-0.10386	
486.38	146B (trif)	152B (Fe)	-0.10892	0.0015
	146B (trif)	153B (Fe)	0.96860	
	147B (pyclen)	154B (Fe)	-0.16289	
485.02	142B (trif)	152B (Fe)	-0.11480	0.0000
	143B (trif)	152B (Fe)	-0.12185	
	145B (trif)	153B (Fe)	0.94115	
	147B (pyclen)	154B (Fe)	0.20396	
	148B (pyclen)	153B (Fe)	-0.10574	
471.37	142B (trif)	152B (Fe)	0.54593	0.0003
	142B (trif)	153B (Fe)	0.20487	
	143B (trif)	152B (Fe)	0.65019	
	143B (trif)	153B (Fe)	0.19735	
	144B (trif)	152B (Fe)	-0.18170	
	145B (trif)	152B (Fe)	0.22802	
	145B (trif)	153B (Fe)	0.17409	
	151B (trif)	155B (Fe)	-0.14862	
460.52	146B (trif)	154B (Fe)	0.99228	0.0011
459.42	142B (trif)	152B (Fe)	0.10454	0.0006
	143B (trif)	152B (Fe)	0.14909	
	144B (trif)	152B (Fe)	0.97517	
456.83	144B (trif)	153B (Fe)	-0.13855	0.0009
	145B (trif)	154B (Fe)	0.95661	
452.63	144B (trif)	153B (Fe)	0.97883	0.0015
	145B (trif)	154B (Fe)	0.13797	
445.92	141B (trif)	152B (Fe)	-0.10575	0.0002
	142B (trif)	152B (Fe)	0.70305	

	142B (trif)	153B (Fe)	-0.25968	
	143B (trif)	152B (Fe)	-0.35775	
	143B (trif)	153B (Fe)	-0.49195	
	147B (pyclen)	154B (Fe)	0.12208	
	151B (trif)	155B (Fe)	0.13535	
443.07	141B (trif)	152B (Fe)	0.16959	0.0025
	142B (trif)	152B (Fe)	0.33070	
	142B (trif)	153B (Fe)	0.23129	
	143B (trif)	152B (Fe)	-0.57111	
	143B (trif)	153B (Fe)	0.59638	
	147B (pyclen)	154B (Fe)	-0.10315	
	151B (trif)	155B (Fe)	-0.31103	
441.83	142B (trif)	152B (Fe)	0.10513	0.0016
	142B (trif)	153B (Fe)	0.12411	
	143B (trif)	153B (Fe)	0.33705	
	143B (trif)	154B (Fe)	0.10682	
	145B (trif)	154B (Fe)	0.14133	
	151B (trif)	155B (Fe)	0.89004	
437.52	142B (trif)	153B (Fe)	0.88365	0.0008
	143B (trif)	152B (Fe)	-0.10923	
	143B (trif)	153B (Fe)	-0.44275	
432.63	141B (trif)	152B (Fe)	0.87377	0.0063
	141B (trif)	153B (Fe)	0.26023	
	142B (trif)	154B (Fe)	-0.11307	
	143B (trif)	152B (Fe)	0.13526	
	143B (trif)	154B (Fe)	-0.16128	
	144B (trif)	154B (Fe)	-0.18999	
	149B (trif)	155B (Fe)	-0.10549	
	151B (trif)	155B (Fe)	0.15844	
430.80	142B (trif)	154B (Fe)	-0.32383	0.0082
	143B (trif)	154B (Fe)	-0.42184	
	144B (trif)	154B (Fe)	0.76083	
	149B (trif)	155B (Fe)	-0.18519	
	150B (pyclen)	155B (Fe)	0.22387	
	151B (trif)	155B (Fe)	0.11841	
428.27	141B (trif)	152B (Fe)	0.22265	0.0042
	141B (trif)	153B (Fe)	0.20125	
	142B (trif)	154B (Fe)	0.36696	
	143B (trif)	154B (Fe)	0.43999	
	144B (trif)	154B (Fe)	0.57632	
	149B (trif)	155B (Fe)	0.13274	
	150B (pyclen)	155B (Fe)	-0.46500	
424.77	141B (trif)	152B (Fe)	0.27325	0.0110
	141B (trif)	153B (Fe)	-0.52411	
	142B (trif)	154B (Fe)	0.14139	
	143B (trif)	154B (Fe)	0.32235	
	144B (trif)	154B (Fe)	0.19583	
	149B (trif)	155B (Fe)	0.21060	
	150B (pyclen)	155B (Fe)	0.64118	
424.24	142B (trif)	154B (Fe)	-0.65403	0.0005
	143B (trif)	154B (Fe)	0.66381	
	149B (trif)	155B (Fe)	-0.33076	
415.26	141B (trif)	153B (Fe)	0.11116	0.0033
	142B (trif)	154B (Fe)	-0.45385	
	149B (trif)	155B (Fe)	0.86839	
407.60	140B (trif+pyclen)	152B (Fe)	-0.43143	0.0008
	141B (trif)	154B (Fe)	0.88945	

405.35	140B (trif+pyclen)	152B (Fe)	0.84458	0.0053
	140B (trif+pyclen)	153B (Fe)	0.28525	
	141B (trif)	154B (Fe)	0.40261	
397.99	140B (trif+pyclen)	152B (Fe)	-0.23504	0.0255
	140B (trif+pyclen)	153B (Fe)	0.86094	
	151B (trif)	156B (Fe)	-0.39326	
394.33	140B (trif+pyclen)	153B (Fe)	0.36909	0.0111
	151B (trif)	156B (Fe)	0.91205	
383.47	139B (trif)	152B (Fe)	0.13700	0.0020
	140B (trif+pyclen)	154B (Fe)	0.59184	
	149B (trif)	156B (Fe)	0.16736	
	150B (pyclen)	156B (Fe)	0.75984	
383.01	140B (trif+pyclen)	154B (Fe)	0.76489	0.0010
	150B (pyclen)	156B (Fe)	-0.63122	
377.86	139B (trif)	152B (Fe)	0.77193	0.0061
	139B (trif)	153B (Fe)	0.20920	
	140B (trif+pyclen)	154B (Fe)	-0.19213	
	148B (pyclen)	155B (Fe)	-0.10183	
	149B (trif)	156B (Fe)	0.51063	
	150B (pyclen)	156B (Fe)	-0.13604	
374.47	139B (trif)	152B (Fe)	-0.54327	0.0058
	147B (pyclen)	155B (Fe)	-0.17789	
	148B (pyclen)	155B (Fe)	0.12132	
	149B (trif)	156B (Fe)	0.80059	
372.32	138B (pyclen)	152B (Fe)	0.72912	0.0088
	138B (pyclen)	153B (Fe)	-0.26507	
	139B (trif)	153B (Fe)	-0.57056	
	148B (pyclen)	155B (Fe)	-0.19103	
370.82	138B (pyclen)	152B (Fe)	0.45806	0.0419
	139B (trif)	153B (Fe)	0.36012	
	148B (pyclen)	155B (Fe)	0.75319	
	148B (pyclen)	156B (Fe)	-0.18898	
	149B (trif)	156B (Fe)	-0.11589	
367.79	138B (pyclen)	152B (Fe)	0.38275	0.0014
	138B (pyclen)	153B (Fe)	0.82843	
	139B (trif)	153B (Fe)	0.17483	
	139B (trif)	154B (Fe)	-0.10194	
	145B (trif)	155B (Fe)	0.10497	
	147B (pyclen)	155B (Fe)	-0.10238	
	148B (pyclen)	155B (Fe)	-0.23508	
366.09	138B (pyclen)	152B (Fe)	0.22172	0.0144
	138B (pyclen)	153B (Fe)	-0.47574	
	139B (trif)	152B (Fe)	-0.11458	
	139B (trif)	153B (Fe)	0.60124	
	145B (trif)	155B (Fe)	0.21993	
	147B (pyclen)	155B (Fe)	-0.15417	
	148B (pyclen)	155B (Fe)	-0.37104	
	148B (pyclen)	156B (Fe)	0.22811	
364.59	138B (pyclen)	152B (Fe)	0.13955	0.0711
	139B (trif)	152B (Fe)	-0.11468	
	139B (trif)	154B (Fe)	-0.22475	
	140B (trif+pyclen)	154B (Fe)	-0.1107	
	147B (pyclen)	155B (Fe)	0.90452	
	147B (pyclen)	156B (Fe)	0.13796	
	149B (trif)	156B (Fe)	0.11485	

356.75	138B (pyclen)	152B (Fe)	0.12311	0.0047
	139B (trif)	154B (Fe)	0.94457	
	145B (trif)	155B (Fe)	0.13235	
	147B (pyclen)	155B (Fe)	0.17823	
	147B (pyclen)	156B (Fe)	0.11304	
350.58	138B (pyclen)	154B (Fe)	0.94285	0.0007
	145B (trif)	155B (Fe)	-0.15496	
	147B (pyclen)	156B (Fe)	0.20784	
349.31	146B (trif)	155B (Fe)	0.99147	0.0007
346.32	137B (pyclen)	152B (Fe)	0.99135	0.0002
	148B (pyclen)	156B (Fe)	-0.10550	
344.49	155A (Fe+pyclen)	157A (pyclen)	0.10482	0.0238
	156A (Fe+pyclen)	157A (pyclen)	0.10845	
	137B (pyclen)	152B (Fe)	-0.10110	
	137B (pyclen)	153B (Fe)	-0.13700	
	138B (pyclen)	154B (Fe)	0.15674	
	139B (trif)	154B (Fe)	-0.11364	
	145B (trif)	155B (Fe)	0.67566	
	148B (pyclen)	156B (Fe)	-0.64511	
342.40	137B (pyclen)	153B (Fe)	0.96620	0.0004
	145B (trif)	155B (Fe)	0.21337	
340.41	156A (Fe+pyclen)	157A (pyclen)	0.61094	0.0173
	137B (pyclen)	153B (Fe)	0.11711	
	138B (pyclen)	154B (Fe)	0.12585	
	142B (trif)	155B (Fe)	-0.11359	
	143B (trif)	155B (Fe)	-0.13840	
	145B (trif)	155B (Fe)	-0.28813	
	147B (pyclen)	155B (Fe)	0.11770	
	147B (pyclen)	156B (Fe)	-0.60496	
	148B (pyclen)	156B (Fe)	-0.25335	
340.07	156A (Fe+pyclen)	157A (pyclen)	0.53182	0.0190
	137B (pyclen)	153B (Fe)	0.11374	
	138B (pyclen)	154B (Fe)	-0.17964	
	145B (trif)	155B (Fe)	-0.21569	
	147B (pyclen)	155B (Fe)	-0.12378	
	147B (pyclen)	156B (Fe)	0.73202	
	148B (pyclen)	156B (Fe)	-0.16586	
335.90	155A (Fe+pyclen)	157A (pyclen)	-0.46481	0.0237
	156A (Fe+pyclen)	157A (pyclen)	0.53684	
	137B (pyclen)	153B (Fe)	-0.11362	
	142B (trif)	155B (Fe)	0.20467	
	143B (trif)	155B (Fe)	0.23091	
	145B (trif)	155B (Fe)	0.35194	
	148B (pyclen)	155B (Fe)	0.18285	
	148B (pyclen)	156B (Fe)	0.43138	
332.04	155A (Fe+pyclen)	157A (pyclen)	-0.54758	0.0067
	136B (trif+pyclen)	152B (Fe)	-0.11685	
	144B (trif)	155B (Fe)	0.78869	
	148B (pyclen)	156B (Fe)	-0.17347	
331.69	155A (Fe+pyclen)	157A (pyclen)	0.62472	0.0137
	156A (Fe+pyclen)	157A (pyclen)	0.13524	
	136B (trif+pyclen)	152B (Fe)	0.25522	
	142B (trif)	155B (Fe)	0.14879	
	143B (trif)	155B (Fe)	0.18108	
	144B (trif)	155B (Fe)	0.60099	
	145B (trif)	155B (Fe)	0.13812	

	148B (pyclen)	155B (Fe)	0.10520	
	148B (pyclen)	156B (Fe)	0.24426	
330.41	155A (Fe+pyclen)	157A (pyclen)	-0.22523	0.0076
	136B (trif+pyclen)	152B (Fe)	0.93077	
	136B (trif+pyclen)	153B (Fe)	-0.17228	
	148B (pyclen)	156B (Fe)	-0.15924	
329.11	137B (pyclen)	154B (Fe)	0.99939	0.0000
326.98	135B (trif)	152B (Fe)	-0.12640	0.0031
	136B (trif+pyclen)	152B (Fe)	0.15658	
	136B (trif+pyclen)	153B (Fe)	0.95881	
	143B (trif)	155B (Fe)		
324.14	135B (trif)	152B (Fe)	0.11635	0.0003
	142B (trif)	155B (Fe)	-0.67585	
	143B (trif)	155B (Fe)	0.71929	
322.73	135B (trif)	152B (Fe)	0.92081	0.0062
	136B (trif+pyclen)	153B (Fe)	0.10342	
	142B (trif)	155B (Fe)	0.24741	
	145B (trif)	156B (Fe)	0.13235	
	146B (trif)	156B (Fe)	0.13845	
319.88	133B (trif)	152B (Fe)	-0.12557	0.0019
	135B (trif)	153B (Fe)	0.93221	
	141B (trif)	155B (Fe)	0.10478	
	142B (trif)	155B (Fe)	0.16341	
	145B (trif)	156B (Fe)	0.16506	
318.28	134B (trif)	152B (Fe)	-0.12751	0.0253
	136B (trif+pyclen)	154B (Fe)	0.10536	
	141B (trif)	155B (Fe)	-0.30155	
	142B (trif)	155B (Fe)	-0.12400	
	145B (trif)	156B (Fe)	-0.20342	
	146B (trif)	156B (Fe)	0.88680	
318.03	141B (trif)	155B (Fe)	0.92432	0.0046
	145B (trif)	156B (Fe)	-0.17905	
	146B (trif)	156B (Fe)	0.26782	
317.23	135B (trif)	152B (Fe)	-0.24332	0.0037
	135B (trif)	153B (Fe)	-0.24961	
	142B (trif)	155B (Fe)	0.20786	
	143B (trif)	155B (Fe)	0.18019	
	145B (trif)	156B (Fe)	0.82953	
	146B (trif)	156B (Fe)	0.25782	
314.63	133B (trif)	152B (Fe)	0.24968	0.0007
	136B (trif+pyclen)	154B (Fe)	0.93373	
	141B (trif)	155B (Fe)	0.11059	
	145B (trif)	156B (Fe)	0.14480	
313.93	133B (trif)	152B (Fe)	-0.48208	0.0010
	134B (trif)	152B (Fe)	0.82711	
	135B (trif)	153B (Fe)	-0.12705	
	136B (trif+pyclen)	154B (Fe)	0.16630	
313.00	146A (trif+pyclen)	157A (pyclen)	0.18160	0.0003
	152A (trif+pyclen)	157A (pyclen)	-0.35625	
	152A (trif+pyclen)	158A (pyclen)	-0.44290	
	153A (trif)	157A (pyclen)	-0.20477	
	153A (trif)	158A (pyclen)	-0.23372	
	154A (trif)	157A (pyclen)	-0.11400	
	140B (trif+pyclen)	157B (pyclen)	-0.13007	
	141B (trif)	157B (pyclen)	-0.11794	

	150B (pyclen)	157B (pyclen)	0.38125	
	150B (pyclen)	158B (pyclen)	0.49635	
312.21	133B (trif)	152B (Fe)	0.72651	0.0037
	133B (trif)	153B (Fe)	-0.19331	
	134B (trif)	152B (Fe)	0.48352	
	134B (trif)	153B (Fe)	-0.35542	
	136B (trif+pyclen)	154B (Fe)	-0.14496	
310.15	146A (trif+pyclen)	157A (pyclen)	-0.12450	0.0008
	152A (trif+pyclen)	157A (pyclen)	-0.47883	
	152A (trif+pyclen)	158A (pyclen)	0.30871	
	153A (trif)	157A (pyclen)	-0.31972	
	153A (trif)	158A (pyclen)	0.16552	
	154A (trif)	157A (pyclen)	-0.10582	
	133B (trif)	153B (Fe)	-0.11961	
	150B (pyclen)	157B (pyclen)	0.53049	
	150B (pyclen)	158B (pyclen)	-0.34838	
309.74	133B (trif)	153B (Fe)	0.66153	0.0107
	134B (trif)	153B (Fe)	-0.52778	
	135B (trif)	154B (Fe)	-0.24289	
	142B (trif)	155B (Fe)	-0.22272	
	142B (trif)	156B (Fe)	-0.12459	
	143B (trif)	155B (Fe)	-0.20357	
	143B (trif)	156B (Fe)	-0.14095	
	145B (trif)	156B (Fe)	0.10161	
	150B (pyclen)	158B (pyclen)	-0.12052	
308.57	133B (trif)	152B (Fe)	0.26355	0.0020
	133B (trif)	153B (Fe)	0.63015	
	134B (trif)	152B (Fe)	0.16402	
	134B (trif)	153B (Fe)	0.56960	
	135B (trif)	154B (Fe)	0.39662	
307.50	131B (trif)	153B (Fe)	-0.12786	0.0077
	132B (pyclen)	152B (Fe)	-0.10540	
	133B (trif)	153B (Fe)	-0.21877	
	133B (trif)	154B (Fe)	0.11176	
	135B (trif)	154B (Fe)	0.62125	
	136B (trif+pyclen)	154B (Fe)	-0.11708	
	140B (trif+pyclen)	155B (Fe)	-0.13166	
	142B (trif)	155B (Fe)	-0.21533	
	142B (trif)	156B (Fe)	-0.30317	
	143B (trif)	155B (Fe)	-0.19979	
	143B (trif)	156B (Fe)	-0.36592	
	144B (trif)	156B (Fe)	0.24113	
	145B (trif)	156B (Fe)	0.19070	
304.96	132B (pyclen)	152B (Fe)	0.22503	0.0024
	134B (trif)	153B (Fe)	0.22036	
	135B (trif)	154B (Fe)	-0.32012	
	144B (trif)	156B (Fe)	0.87522	
304.80	132B (pyclen)	152B (Fe)	0.95697	0.0016
	135B (trif)	154B (Fe)	0.12150	
	144B (trif)	156B (Fe)	-0.17712	
303.78	131B (trif)	153B (Fe)	0.11346	0.0018
	133B (trif)	152B (Fe)	-0.18726	
	133B (trif)	153B (Fe)	0.12281	
	134B (trif)	153B (Fe)	-0.36532	
	134B (trif)	154B (Fe)	-0.10338	
	135B (trif)	154B (Fe)	0.45476	
	136B (trif+pyclen)	154B (Fe)	0.14585	
	140B (trif+pyclen)	155B (Fe)	0.46312	
	141B (trif)	156B (Fe)	-0.13611	

	142B (trif)	155B (Fe)	0.15100	
	142B (trif)	156B (Fe)	0.14649	
	143B (trif)	155B (Fe)	0.14601	
	143B (trif)	156B (Fe)	0.21308	
	144B (trif)	156B (Fe)	0.35209	
	145B (trif)	156B (Fe)	-0.16046	
302.31	131B (trif)	152B (Fe)	-0.15239	0.0042
	132B (pyclen)	153B (Fe)	-0.10337	
	134B (trif)	153B (Fe)	0.14404	
	134B (trif)	154B (Fe)	0.17438	
	135B (trif)	154B (Fe)	-0.18838	
	140B (trif+pyclen)	155B (Fe)	0.84169	
	141B (trif)	156B (Fe)	0.11882	
	142B (trif)	156B (Fe)	-0.15287	
	143B (trif)	156B (Fe)	-0.23683	
302.09	132B (pyclen)	153B (Fe)	0.97490	0.0002
	140B (trif+pyclen)	155B (Fe)	0.12924	
299.74	130B (trif)	153B (Fe)	-0.11659	0.0019
	131B (trif)	152B (Fe)	0.78375	
	131B (trif)	153B (Fe)	-0.36623	
	132B (pyclen)	153B (Fe)	-0.10341	
	133B (trif)	154B (Fe)	-0.18032	
	134B (trif)	154B (Fe)	-0.33731	
	140B (trif+pyclen)	155B (Fe)	0.13084	
	142B (trif)	156B (Fe)	-0.13720	
298.49	131B (trif)	152B (Fe)	0.22465	0.0007
	131B (trif)	153B (Fe)	0.23280	
	133B (trif)	154B (Fe)	0.33054	
	134B (trif)	154B (Fe)	0.15509	
	141B (trif)	156B (Fe)	0.13852	
	142B (trif)	156B (Fe)	-0.55710	
	143B (trif)	156B (Fe)	0.63653	
298.12	130B (trif)	152B (Fe)	-0.12413	0.0012
	131B (trif)	152B (Fe)	0.53191	
	131B (trif)	153B (Fe)	0.31425	
	133B (trif)	154B (Fe)	0.19945	
	134B (trif)	154B (Fe)	0.55362	
	142B (trif)	156B (Fe)	0.43597	
	143B (trif)	156B (Fe)	-0.20639	
298.02	154A (trif)	157A (pyclen)	0.15424	0.0011
	131B (trif)	153B (Fe)	0.18436	
	133B (trif)	154B (Fe)	0.68822	
	134B (trif)	154B (Fe)	-0.60691	
	141B (trif)	156B (Fe)	0.12243	
	142B (trif)	156B (Fe)	0.19175	
	143B (trif)	156B (Fe)	-0.17373	
296.40	154A (trif)	157A (pyclen)	0.56306	0.0117
	130B (trif)	152B (Fe)	0.23915	
	131B (trif)	153B (Fe)	0.56768	
	133B (trif)	154B (Fe)	-0.35962	
	142B (trif)	156B (Fe)	-0.23115	
	143B (trif)	156B (Fe)	-0.23827	
295.79	152A (trif+pyclen)	157A (pyclen)	-0.10334	0.0103
	154A (trif)	157A (pyclen)	0.78497	
	130B (trif)	152B (Fe)	-0.18038	
	131B (trif)	153B (Fe)	-0.44507	
	134B (trif)	154B (Fe)	0.16235	
	142B (trif)	156B (Fe)	0.17501	
	143B (trif)	156B (Fe)	0.18247	

294.77	130B (trif)	152B (Fe)	0.87138	0.0041
	131B (trif)	153B (Fe)	-0.12384	
	134B (trif)	154B (Fe)	0.11142	
	141B (trif)	156B (Fe)	0.34695	
	142B (trif)	156B (Fe)	0.20495	
	143B (trif)	156B (Fe)	0.14056	
292.97	130B (trif)	152B (Fe)	-0.19448	0.0066
	130B (trif)	153B (Fe)	0.69588	
	131B (trif)	153B (Fe)	-0.10950	
	132B (pyclen)	154B (Fe)	-0.24277	
	133B (trif)	154B (Fe)	-0.22298	
	134B (trif)	154B (Fe)	-0.11756	
	141B (trif)	156B (Fe)	0.56153	
292.54	156A (Fe+pyclen)	158A (pyclen)	0.55201	0.0024
	130B (trif)	152B (Fe)	-0.18047	
	130B (trif)	153B (Fe)	-0.53028	
	131B (trif)	153B (Fe)	0.12024	
	132B (pyclen)	154B (Fe)	-0.32490	
	133B (trif)	154B (Fe)	-0.15323	
	141B (trif)	156B (Fe)	0.42234	
	142B (trif)	156B (Fe)	0.13065	
	143B (trif)	156B (Fe)	0.10662	
292.41	156A (Fe+pyclen)	158A (pyclen)	0.83047	0.0010
	130B (trif)	153B (Fe)	0.39512	
	131B (trif)	153B (Fe)	-0.10025	
	132B (pyclen)	154B (Fe)	0.20329	
	141B (trif)	156B (Fe)	-0.24291	
290.84	130B (trif)	152B (Fe)	-0.15322	0.0095
	131B (trif)	153B (Fe)	0.10642	
	131B (trif)	154B (Fe)	-0.16709	
	132B (pyclen)	154B (Fe)	0.86685	
	133B (trif)	154B (Fe)	-0.14419	
	141B (trif)	156B (Fe)	0.33721	

Coordinates of optimized geometries (ANG), “xyz” format.

$[FeCl_2(pyclen)]^+$ / OPBE / 6-31G(d,p) / gas phase

36
36

Fe	0.929617	0.000209	0.513379
N	-1.205846	0.000048	0.224970
N	0.419114	-2.113547	0.016737
N	0.928341	-0.000874	-1.789593
N	0.418987	2.113499	0.014747
Cl	3.152271	0.000065	0.313214
Cl	0.607375	0.001798	2.704934
C	-1.861357	1.169166	0.171972
C	-1.861300	-1.169133	0.173085
C	-0.988233	-2.386439	0.367133
C	0.787344	-2.393483	-1.389913
H	1.008553	-2.689864	0.617051
C	0.370000	-1.251135	-2.309834
C	0.369900	1.248842	-2.311019
H	1.936868	-0.000903	-1.950908
C	0.787172	2.392095	-1.392188
C	-0.988347	2.386677	0.364943
H	1.008443	2.690387	0.614497
C	-3.250384	1.209962	0.030766
C	-3.250336	-1.210129	0.031949
H	-1.019115	-2.643769	1.436108
H	-1.383915	-3.250981	-0.185992
H	0.345368	-3.339784	-1.737672
H	1.878248	-2.513005	-1.415727
H	0.705298	-1.468471	-3.336597
H	-0.722265	-1.159163	-2.344913
H	0.705177	1.465229	-3.337991
H	-0.722357	1.156755	-2.346002
H	0.345121	3.338026	-1.740854
H	1.878066	2.511673	-1.418136
H	-1.384073	3.250756	-0.188874
H	-1.019179	2.644869	1.433712
H	-3.777247	2.161538	-0.016256
C	-3.945315	-0.000137	-0.042717
H	-3.777156	-2.161775	-0.014129
H	-5.028912	-0.000213	-0.156773

$[FeCl_2(pyclen)]^+$ / OPBE / 6-31G(d,p) / solvent

36

36

Fe	0.906901	-0.009749	0.445560
N	-1.215867	0.001834	0.253725
N	0.396806	-2.099561	-0.037539
N	0.913464	0.018699	-1.799095
N	0.413336	2.096089	0.018691
Cl	3.207881	0.007003	0.361008
Cl	0.687219	-0.060951	2.734820
C	-1.866379	1.176765	0.222504
C	-1.875764	-1.166490	0.190046
C	-1.008436	-2.390554	0.310040
C	0.758429	-2.372461	-1.448112
H	0.984863	-2.691213	0.551238
C	0.339068	-1.219194	-2.342625
C	0.346580	1.274565	-2.308432
H	1.912611	0.018527	-2.013268
C	0.774711	2.401940	-1.385507
C	-0.988779	2.389742	0.376053
H	1.007510	2.667526	0.621100
C	-3.257408	1.222383	0.111816
C	-3.267227	-1.197793	0.078568
H	-1.033349	-2.724918	1.356342
H	-1.406985	-3.212126	-0.300261
H	0.301622	-3.311190	-1.792334
H	1.847550	-2.499522	-1.480539
H	0.678781	-1.404115	-3.372397
H	-0.751807	-1.119034	-2.370401
H	0.685379	1.483982	-3.333829
H	-0.744947	1.182367	-2.336289
H	0.323043	3.351911	-1.704908
H	1.864514	2.522663	-1.416786
H	-1.380740	3.231516	-0.210462
H	-1.009954	2.694558	1.431493
H	-3.774787	2.179469	0.079021
C	-3.957772	0.015865	0.039656
H	-3.792192	-2.149466	0.019489
H	-5.043544	0.021621	-0.055378

$[FeBr_2(pyclen)]^+$ / OPBE / 6-31G(d,p) / gas phase

36

36

Fe	-0.611960	0.192945	0.000113
N	1.540779	0.038348	-0.000064
N	-0.067702	-0.277217	-2.113192
N	-0.455606	-2.115246	0.000145
N	-0.067407	-0.277050	2.113312
Br	-2.931020	-0.160982	0.000006
Br	-0.375495	2.511964	-0.000042
C	2.198390	0.043442	1.168872
C	2.198233	0.043340	-1.169082
C	1.314286	0.160334	-2.388980
C	-0.342921	-1.704951	-2.392338
H	-0.697670	0.285505	-2.684543
C	0.136137	-2.595114	-1.249930
C	0.136399	-2.595009	1.250116
H	-1.450490	-2.347848	0.000272
C	-0.342484	-1.704802	2.392569
C	1.314595	0.160588	2.388865
H	-0.697333	0.285647	2.684734
C	3.594413	0.024905	1.209600
C	3.594251	0.024822	-1.209994
H	1.279425	1.223773	-2.668013
H	1.746959	-0.382105	-3.242681
H	0.121361	-2.023609	-3.338477
H	-1.429559	-1.804982	-2.511837
H	-0.129426	-3.642086	-1.468363
H	1.228499	-2.557309	-1.159054
H	-0.129085	-3.641976	1.468681
H	1.228747	-2.557181	1.159027
H	0.122026	-2.023388	3.338618
H	-1.429087	-1.804925	2.512304
H	1.747400	-0.381696	3.242600
H	1.279725	1.224071	2.667730
H	4.123625	0.025291	2.161096
C	4.293266	0.012387	-0.000245
H	4.123337	0.025205	-2.161560
H	5.382690	-0.004840	-0.000320

$[FeBr_2(pyclen)]^+$ / OPBE / 6-31G(d,p) / solvent

36

36

Fe	0.586351	0.136409	-0.000042
N	-1.550953	0.067297	0.000095
N	0.048618	-0.302887	2.106291
N	0.427073	-2.129868	-0.000116
N	0.048334	-0.302743	-2.106340
Br	2.959163	-0.151896	-0.000127
Br	0.437781	2.518002	0.000017
C	-2.207585	0.085792	-1.170820
C	-2.207439	0.085667	1.171093
C	-1.328564	0.146801	2.392416
C	0.303089	-1.735274	2.390324
H	0.673876	0.240696	2.702326
C	-0.179537	-2.612006	1.246613
C	-0.179814	-2.611897	-1.246752
H	1.406673	-2.419633	-0.000238
C	0.302661	-1.735130	-2.390500
C	-1.328855	0.147062	-2.392241
H	0.673550	0.240834	-2.702425
C	-3.603336	0.106957	-1.209881
C	-3.603185	0.106830	1.210330
H	-1.279496	1.193695	2.723803
H	-1.771627	-0.427425	3.217227
H	-0.179341	-2.037796	3.331231
H	1.386343	-1.849921	2.523061
H	0.087070	-3.660389	1.448978
H	-1.270003	-2.567338	1.149790
H	0.086685	-3.660287	-1.449230
H	-1.270258	-2.567162	-1.149712
H	-0.179954	-2.037568	-3.331339
H	1.385885	-1.849836	-2.523434
H	-1.772048	-0.427018	-3.217085
H	-1.279771	1.194004	-2.723476
H	-4.127251	0.113072	-2.164050
C	-4.301090	0.115549	0.000269
H	-4.126983	0.112845	2.164565
H	-5.391103	0.124195	0.000338

$[Fe(OTf)_2(pyclen)]^+$ / OPBE / 6-31G(d,p) / gas phase

59
59

Fe	0.170997	-0.546794	0.024079
N	2.275572	-0.889195	-0.043692
N	0.582716	-0.975245	-2.166272
N	0.004575	-2.880888	0.008839
N	0.721682	-1.006750	2.177384
C	2.970096	-0.990977	1.102431
C	2.893650	-0.957317	-1.235367
C	2.011189	-0.676877	-2.420315
C	0.265442	-2.407132	-2.401311
C	-0.254080	-0.124939	-3.048852
C	0.671141	-3.305074	-1.242300
C	0.727495	-3.324600	1.221947
C	-1.377615	-3.407610	0.037103
C	0.385868	-2.434809	2.407191
C	2.169608	-0.745729	2.351884
C	-0.043536	-0.156088	3.123611
H	-1.947407	-3.044678	-0.818905
C	4.350436	-1.203796	1.093180
C	4.270353	-1.170374	-1.323078
H	2.098461	0.401065	-2.614144
H	2.369411	-1.198638	-3.320638
H	0.746232	-2.760967	-3.327481
H	-0.814833	-2.475805	-2.568102
H	-0.054202	0.928742	-2.839499
H	-1.311073	-0.314353	-2.849799
H	-0.042771	-0.330693	-4.108922
H	0.418365	-4.348231	-1.493617
H	1.755118	-3.275237	-1.093603
H	0.476839	-4.367986	1.474046
H	1.803653	-3.303597	1.021493
H	-1.904099	-3.063019	0.927881
H	-1.368166	-4.508572	0.025400
H	0.895504	-2.809291	3.309555
H	-0.688403	-2.483580	2.615532
H	2.573004	-1.312441	3.204670
H	2.290592	0.320910	2.586489
H	-1.114801	-0.304967	2.971908
H	0.184757	0.895600	2.934996
H	0.212988	-0.399450	4.165541
H	4.903714	-1.283766	2.027088
C	5.000623	-1.297112	-0.139109
H	4.761300	-1.224764	-2.292955
H	6.076810	-1.463386	-0.176982
O	-2.864131	1.416257	-1.039427
F	-5.469572	0.106136	-0.084742

F	-4.231700	-1.267425	-1.239841
C	-4.351956	-0.608014	-0.078592
S	-2.890655	0.556091	0.140189
O	-2.983337	1.111157	1.488180
F	-4.387064	-1.493733	0.923951
O	-1.727511	-0.514283	0.073303
O	0.442537	1.330361	0.000835
F	-0.334131	3.911790	-1.261881
F	-0.633366	3.911126	0.898657
C	0.268068	3.970508	-0.076329
S	1.462937	2.521891	0.081233
O	2.322315	2.531466	-1.105670
F	0.972908	5.094293	0.020605
O	2.058924	2.580111	1.419547

$[Fe(OTf)_2(pyclen)]^+$ / OPBE / 6-31G(d,p) / solvent

59
59

Fe	-0.217415	-0.609768	0.046201
N	-2.295032	-0.857586	-0.066248
N	-0.837030	-0.684257	2.218893
N	-0.093569	-2.848549	0.426296
N	-0.529681	-1.376821	-2.060531
C	-2.871833	-1.168895	-1.240689
C	-3.028638	-0.731252	1.056330
C	-2.265095	-0.288560	2.268746
C	-0.633750	-2.079140	2.702018
C	-0.047533	0.239342	3.063410
C	-0.922927	-3.106116	1.628529
C	-0.653942	-3.510097	-0.778531
C	1.286578	-3.333459	0.658456
C	-0.166349	-2.820249	-2.033246
C	-1.953659	-1.175847	-2.426787
C	0.325315	-0.683660	-3.051098
H	1.748873	-2.803147	1.492219
C	-4.248057	-1.385179	-1.330608
C	-4.408088	-0.933978	1.039517
H	-2.311632	0.807943	2.300568
H	-2.737654	-0.655538	3.189561
H	-1.268432	-2.269032	3.579537
H	0.405943	-2.158311	3.034508
H	-0.149223	1.262368	2.695630
H	1.005436	-0.049864	3.034015
H	-0.397280	0.197798	4.105563
H	-0.719210	-4.111923	2.025800
H	-1.977758	-3.085758	1.340072
H	-0.355073	-4.568513	-0.807356
H	-1.746534	-3.491796	-0.720012
H	1.902805	-3.171626	-0.226987
H	1.265029	-4.409715	0.884758
H	-0.574596	-3.326170	-2.920368
H	0.924530	-2.877845	-2.101168
H	-2.271934	-1.920791	-3.168085
H	-2.043841	-0.192926	-2.908307
H	1.377351	-0.839016	-2.802701
H	0.106476	0.386531	-3.046708
H	0.138324	-1.082031	-4.059490
H	-4.699171	-1.643102	-2.286727
C	-5.017865	-1.266425	-0.172429
H	-4.985111	-0.836572	1.956977
H	-6.093135	-1.439389	-0.212259
O	3.131720	1.299331	1.250311
F	5.478421	-0.020029	-0.233310

F	4.390127	-1.411761	1.040220
C	4.328906	-0.688081	-0.082960
S	2.924788	0.553193	0.004274
O	2.960188	1.270481	-1.274284
F	4.165176	-1.510790	-1.126022
O	1.724375	-0.415757	0.106946
O	-0.441631	1.369229	-0.188033
F	-0.551678	3.754929	1.614526
F	0.928327	4.010532	0.035918
C	-0.379771	3.959045	0.302029
S	-1.214397	2.600762	-0.687773
O	-2.617532	2.612270	-0.252759
F	-0.938134	5.130796	-0.027710
O	-0.917167	2.900922	-2.094914

Relevant experimental vs theoretical geometrical parameters of $[FeX_2(pyclen)]X$ (X=Cl, Br), **1a** and **1b**

Table S11. Absolute (Å or °) and relative (%) differences between the experimental and the theoretical geometries of **1a** and **1b**. We refer to Table S4 for the meaning of dFeN4, Fe-X_{short}, Fe-X_{long} and X-Fe-X.

Differences theo-exp	X=Cl	X=Br
dFeN4 (gas) (Å)	0.104	0.113
dFeN4 (gas) (%)	10	10
dFeN4 (solv) (Å)	0.055	0.077
dFeN4 (solv) (%)	5	7
Fe-X_{short} (gas) (Å)	-0.065	-0.091
Fe-X_{short} (gas) (%)	-3	-4
Fe-X_{short} (solv) (Å)	0.020	-0.036
Fe-X_{short} (solv) (%)	1	-1
Fe-X_{long} (gas) (Å)	-0.054	-0.089
Fe-X_{long} (gas) (%)	-2	-4
Fe-X_{long} (solv) (Å)	0.017	-0.045
Fe-X_{long} (solv) (%)	1	-2
X-Fe-X (gas-exp) (°)	7.7	8.5
X-Fe-X (solv-exp) (°)	1.8	4.5

Stability of radicals involved in the homolytic Fe-X bond dissociation in **1a**, **1b** and **1c**

Energies in kcal/mole. Data obtained with the 6-31G(d,p) basis set.

H• + Cl• → HCl

Method	gas phase	gas + ZPE	solvent	solvent + ZPE
DFT/OPBE	-106.8	-102.5	-108.5	-104.2
CCSD	-97.4		-98.7	
CISD	-95.5	-91.1	-96.9	-92.5

H• + Br• → HBr

Method	gas phase	gas + ZPE	solvent	solvent + ZPE
DFT/OPBE	-96.0	-92.1	-97.0	-93.1
CCSD	-88.1		-89.0	
CISD	-80.5	-76.6	-81.5	-77.6

H• + OTf• → HOTf

Method	gas phase	gas + ZPE	solvent	solvent + ZPE
DFT/OPBE	*-103.6*	*-95.3*	*-107.8*	*-99.7*
CCSD	-113.9		-118.6	
CISD	-108.9	-100.6	-113.5	-105.2

We report in italic (OPBE) data affected by high instability in the convergence procedure.

CCSD: Coupled Cluster with singles and doubles

CISD: Configurations Interaction with single and double excitations

References

(1) Dellacqua, M.; Castano, B.; Cecchini, C.; Pedrazzini, T.; Pirovano, V.; Rossi, E.; Caselli, A.; Abbiati, G. Mild Regiospecific Synthesis of 1-Alkoxy-Isochromenes Catalyzed by Well-Defined [Silver(I)(Pyridine-Containing Ligand)] Complexes. *J. Org. Chem.* 2014, **79 (8)**, 3494–3505. https://doi.org/10.1021/jo5002559.

(2) Haynes, J. S.; Sams, J. R.; Thompson, R. C. Synthesis and Structural Studies of Iron(II) and Iron(III) Sulfonates. *Can. J. Chem.* 1981, **59 (4)**, 669–678. https://doi.org/10.1139/v81-098.

(3) Serrano-Plana, J.; Aguinaco, A.; Belda, R.; García-España, E.; Basallote, M. G.; Company, A.; Costas, M. Exceedingly Fast Oxygen Atom Transfer to Olefins via a Catalytically Competent Nonheme Iron Species. *Angew. Chem., Int. Ed.* 2016, **55 (21)**, 6310–6314. https://doi.org/10.1002/ANIE.201601396.

(4) Panza, N.; di Biase, A.; Rizzato, S.; Gallo, E.; Tseberlidis, G.; Caselli, A. Catalytic Selective Oxidation of Primary and Secondary Alcohols Using Nonheme [Iron(III)(Pyridine-Containing Ligand)] Complexes. *Eur. J. Org. Chem.* 2020, 6635–6644. https://doi.org/10.1002/ejoc.202001201.

(5) Tseberlidis, G.; Demonti, L.; Pirovano, V.; Scavini, M.; Cappelli, S.; Rizzato, S.; Vicente, R.; Caselli, A. Controlling Selectivity in Alkene Oxidation: Anion Driven Epoxidation or Dihydroxylation Catalysed by [Iron(III)(Pyridine-Containing Ligand)] Complexes. *ChemCatChem* 2019, **11 (19)**, 4907–4915. https://doi.org/10.1002/cctc.201901045.

(6) *Handbook of Preparative Inorganic Chemistry,* Vol., 2nd Ed., G. Brauer Ed., Academic press, London, United Kingdom, 1963. https://doi.org/10.1016/B978-0-12-395590-6.X5001-7

(7) *CrysAlis PRO*, CrysAlisPRO, Oxford Diffraction /Agilent Technologies UK Ltd, Yarnton, England, 2019.

(8) Sheldrick, G. M. *SHELXT* – Integrated space-group and crystal-structure determination *Acta Crystallogr. A*, 2015, **71**, 3–8. https://doi.org/10.1107/S2053273314026370.

(9) Farrugia, L. J. WinGX and ORTEP for Windows: An Update. *J. Appl. Crystallogr.* 2012, **45 (4)**, 849–854. https://doi.org/10.1107/S0021889812029111.

(10) Swart, M.; Groenhof, A. R.; Ehlers, A. W.; Lammertsma, K. Validation of Exchange-Correlation Functionals for Spin States of Iron Complexes. *J. Phys. Chem. A*, 2004, **(108)**, 5479–5483.

(11) Swart, M.; Ehlers, A. W.; Lammertsma, K. Performance of the OPBE exchange-correlation functional *Mol. Phys.*, 2004, **102**, 2467–2474.

(12) Marenich, A. V.; Cramer C. J.; Truhlar, D. G. Universal Solvation Model Based on Solute Electron Density and on a Continuum Model of the Solvent Defined by the Bulk Dielectric Constant and Atomic Surface. Tensions *J. Phys. Chem. B*, 2009, **113**, 6378–6396.

(13) Flores-Leonar, M. M.; Moreno-Esparza, R.; Ugalde-Saldívar, V. M.; Amador-Bedolla, C. Correlating Properties in Iron(III) Complexes: A DFT Description of Structure, Redox Potential and Spin Crossover Phenomena. *ChemistrySelect*, 2017, **2**, 4717–4724

(14) Bleda, E. A.; Trindle, C.; Altun, Z. Studies on spin state preferences in Fe(II) complexes. *Comput. Theor. Chem.*, 2015, **1073**, 139–148.

(15) Siig, O. S.; Kepp, K. P. Iron(II) and Iron(III) Spin Crossover: Toward an Optimal Density Functional *J. Phys. Chem. A*, 2018, **122**, 4208–4217.

(16) Diamond - Crystal and Molecular Structure Visualization, Crystal Impact - Dr. H. Putz & Dr. K. Brandenburg GbR, Kreuzherrenstr. 102, 53227 Bonn, Germany, Https://Www.Crystalimpact.de/Diamond.

(17) Nardelli, M. *PARST* 95 – an Update to *PARST* : A System of Fortran Routines for Calculating Molecular Structure Parameters from the Results of Crystal Structure Analyses. *J. Appl. Crystallogr.* 1995, **28 (5)**, 659–659. https://doi.org/10.1107/S0021889895007138.

(18) Bosnich, B.; Poon, C. K.; Tobe, M. L. Complexes of Cobalt(III) with a Cyclic Tetradentate Secondary Amine. *Inorg. Chem.* 1965, **4 (8)**, 1102–1108. https://doi.org/10.1021/IC50030A003/ASSET/IC50030A003.FP.PNG_V03.

(19) Félix, V.; Costa, J.; Delgado, R.; Drew, M. G. B.; Duarte, M. T.; Resende, C. X-Ray Diffraction and Molecular Mechanics Studies of 12-, 13-, and 14-Membered Tetraaza Macrocycles Containing Pyridine: Effect of the Macrocyclic Cavity Size on the Selectivity of the Metal Ion. *J. Chem. Soc., Dalton Trans.* 2001, **9**, 1462–1471. https://doi.org/10.1039/B009773J.

(20) Ketkaew, R.; Tantirungrotechai, Y.; Harding, P.; Chastanet, G.; Guionneau, P.; Marchivie, M.; Harding, D. J. OctaDist: A Tool for Calculating Distortion Parameters in Spin Crossover and Coordination Complexes. *Dalton Trans.* 2021, **50 (3)**, 1086–1096. https://doi.org/10.1039/D0DT03988H.

(21) Holland, J. M.; McAllister, J. A.; Lu, Z.; Kilner, C. A.; Thornton-Pett, M.; Halcrow, M. A. An Unusual Abrupt Thermal Spin-State Transition in [FeL2][BF4]2 [L = 2,6-Di(Pyrazol-1-Yl)Pyridine]. *Chem. Comm.* 2001, **6**, 577–578. https://doi.org/10.1039/B100995H.

(22) Elhaïk, J.; Kilner, C. A.; Halcrow, M. A. An Iron(II) Complex Salt That Crystallises in Three Crystal Forms, One of Which Undergoes a Sterically Controlled Incomplete Spin-State Transition on Cooling. *Cryst. Eng. Comm.* 2005, **7 (23)**, 151–157. https://doi.org/10.1039/B417718E.

(23) Brewer, S. M.; Wilson, K. R.; Jones, D. G.; Reinheimer, E. W.; Archibald, S. J.; Prior, T. J.; Ayala, M. A.; Foster, A. L.; Hubin, T. J.; Green, K. N. Increase of Direct C-C Coupling Reaction Yield by Identifying Structural and Electronic Properties of High-Spin Iron Tetra-Azamacrocyclic Complexes. *Inorg. Chem.* 2018, **57 (15)**, 8890–8902. https://doi.org/10.1021/ACS.INORGCHEM.8B00777/SUPPL_FILE/IC8B00777_SI_001.PDF.

(24) N. W. Alcock, D. H. Busch and C. Y. Liu, *CCDC 639154: Experimental Crystal Structure Determination, 2007, DOI: 10.5517/ccpg2w2*.

(25) Brewer, S. M.; Palacios, P. M.; Johnston, H. M.; Pierce, B. S.; Green, K. N. Isolation and Identification of the Pre-Catalyst in Iron-Catalyzed Direct Arylation of Pyrrole with Phenylboronic Acid. *Inorg. Chim. Acta* 2018, **478**, 139–147. https://doi.org/10.1016/j.ica.2018.03.036.

(26) Brewer, S. M.; Schwartz, T. M.; Mekhail, M. A.; Turan, L. S.; Prior, T. J.; Hubin, T. J.; Janesko, B. G.; Green, K. N. Mechanistic Insights into Iron-Catalyzed C–H Bond Activation and C–C Coupling. *Organometallics* 2021, **40 (15)**, 2467–2477. https://doi.org/10.1021/acs.organomet.1c00211.

(27) Mekhail, M. A.; Pota, K.; Schwartz, T. M.; Green, K. N. Functionalized Pyridine in Pyclen-Based Iron(III) Complexes: Evaluation of Fundamental Properties. *RSC Adv.* 2020, **10 (52)**, 31165–31170. https://doi.org/10.1039/D0RA05756H.

(28) Oliver Kahn, *Molecular magnetism*, VCH, New York, 1993.